Deliverable 8.4:

Principles and performance of NDA systems and innovative detection techniques used for the characterisation of SNF samples and assemblies

Work Package 8

Spent Fuel Characterisation and Evolution until Disposal (SFC)

This project has received funding from the European Union's Horizon 2020 research and innovation programme under grant agreement N°847593.

http://www.ejp-eurad.eu/

Document information

Project Acronym	**EURAD**
Project Title	**European Joint Programme on Radioactive Waste Management**
Project Type	**European Joint Programme (EJP)**
EC grant agreement No.	**847593**
Project starting / end date	**1st June 2019 – 30th May 2024**
Work Package No.	**8**
Work Package Title	**Spent Fuel Characterisation and Evolution until Disposal**
Work Package Acronym	**SFC**
Deliverable No.	**8.4**
Deliverable Title	**Principles and performance of NDA systems and innovative detection techniques used for the characterisation of SNF samples and assemblies**
Lead Beneficiary	**JRC Geel**
Contractual Delivery Date	**31 May 2024**
Actual Delivery Date	**23 May 2024**
Type	
Dissemination level	**PU**
Authors	**Peter Schillebeeckx (EC-JRC), Gery Alaerts (EC-JRC), Alessandro Borella (SCK CEN), Jesper Kirkegaard (Vattenfall), Stefan Kopecky (EC-JRC), Gašper Letnar (JSI), Bent Pedersen (EC-JRC), Pablo Romojaro (SCK CEN) Virginie Solans (UU), Stefano Vaccaro (EC-JRC), Marc Verwerft (SCK CEN), Ruud Wynants (JRC), Gašper Žerovnik (JSI)**

To be cited as:

Schillebeeckx P., Alaerts G., Borella A., Kirkegaard J., Kopecky S., Letnar G., Pedersen B., Romojaro P., Solans V., Vaccaro S., Verwerft M., Wynants R., Žerovnik G. (2024): Spent Fuel Characterisation and Evolution until Disposal. Final version as of 23.05.2024 of deliverable D8.4 of the HORIZON 2020 project EURAD. EC Grant agreement no: 847593.

Disclaimer

Acknowledgement

This document is a deliverable of the European Joint Programme on Radioactive Waste Management (EURAD). EURAD has received funding from the European Union's Horizon 2020 research and innovation programme under grant agreement No 847593.

Status of deliverable		
	By	Date
Delivered (Lead Beneficiary)	P. Schillebeeckx	01/05/2024
Verified (WP Leader)	F. Johansson	22/05/2024
Reviewed (Reviewers)	B. Pedersen V. Solans G. Žerovnik	07/05/2024 07/05/2024 06/05/2024
Approved (PMO)	P. Carbol	23/05/2024
Submitted to EC (Coordinator)	Andra (Coordinator)	04/06/2024

Executive Summary

Procedures to characterise spent fuel for the main observables of interest strongly relies on theoretical calculations using depletion codes which require two types of input data, i.e. nuclear data and design and operational data. To validate the procedures high quality experimental data are required. In this report the principles of methods to characterise spent nuclear fuel by non-destructive assay (NDA) are studied. The focus is on passive NDA methods to produce experimental data for depletion code validation and for the verification of spent fuel related input data.

In section 2 the main observables and radionuclides of interest for NDA of spent fuel without the need of a chemical treatment are discussed. Section 3 describes two NDA methods to produce high quality data for code validation: an absolute method to determine the neutron emission rate of a spent fuel segment sample and calorimetric measurements using calorimeter at the Clab (“Centralt mellanlager för använt kärnbränsle”: Central Interim Storage Facility for Spent Nuclear Fuel) facility. NDA methods to determine characteristics of spent fuel assemblies are discussed in section 4, with an emphasis on measurements using the gamma-ray spectroscopic system installed at Clab and the use of the FORK detector for in-pool measurements to determine the gamma-ray and neutron emission rate of an assembly. The FORK detector is a system that is used by safeguards authorities to verify spent fuel assemblies. It consists of a fission chamber for neutron detection and an ionisation chamber for total gamma-ray detection.

Keywords

Burnup, Calorimetry, Cooling time, Decay heat, Depletion calculations, Fission chamber, Gamma-ray, Initial enrichment, Ionisation chamber, Neutron, Non-destructive assay, Nuclear data, Spent nuclear fuel

Table of content

List of figures

List of Tables

Glossary

BGO	Bismuth Germanate scintillator
BUC	Burnup credit
BU	Burnup
BWR	Boiling water reactor
Clab	Central interim storage facility for spent nuclear fuel in Sweden
CMSYS	Core management system
$CeBr_3$	Cerium Bromide scintillator
CT	Cooling time
CZT	Cadmium Zinc Telluride
DA	Destructive analysis
DDEP	Decay data evaluation project
DDSI	Differential die-away self-interrogation
DOE	Department of energy
EPRI	Electric power research institute
EURAD	European joint programme on radioactive waste management
FC	Fission chamber
HPGe	High purity Germanium detector
HPLC	high performance liquid chromatography
IC	Ionisation chamber
ICP-MS	Inductively coupled plasma mass spectrometry
GE	General electric
IE	Initial enrichment
JRC	Joint research centre
$LaBr_3$	Lanthanum bromide scintillator
LHMA	Laboratory for high and medium level activity
LWR	Light water reactor
MOX	Mixed oxide fuel
NaI	Sodium Iodide scintillator
NGSI-SF	Next generation safeguards initiative – spent fuel
NDA	Non-destructive assay
NPP	Nuclear power plant
PIE	Post irradiation examination
PNAR	Passive neutron albedo reactivity
PWR	Pressurized water reactor
PSI	Paul Scherrer Institute
REGAL	Rod-extremity and gadolinia analysis
SCK CEN	Belgian nuclear research centre
sf	Spontaneous fission
SFC	Spent fuel characterisation and evolution until disposal
SFCOMPO	Spent fuel isotopic composition
SKB	Swedish nuclear fuel and waste management company
SNF	Spent nuclear fuel
UU	Uppsala university

1. Introduction

Characterisation of spent nuclear fuel is required for its safe, economic and ecologic handling, transport, storage and disposal. The main characteristics of interest are neutron and γ-ray emission properties, decay heat, reactivity, long-term radiotoxicity and inventory of mobile long-lived radionuclides. Most of them are hard to measure and depend on a complex inventory of nuclides. Therefore, a reliable estimation of these characteristics can only be determined by calculations using validated depletion codes [1] such as ALEPH2 [2], CASMO5 [3][4], DARWIN [5], EVOLCODE [6], Serpent [7][8], SNF [9] and different modules in the SCALE code system [9] [10].

Al validation of these codes based on experimental data is needed to determine safety margins and procedures for handling, storage and disposal of spent nuclear fuel. Adequate procedures avoid too conservative loading schemes, to avoid the production of over-engineered casks and canisters for storage and disposal and to reduce the volume of underground galleries for geological disposal. Results of depletion calculations strongly depend on the quality of the fuel dependent input data, i.e. design properties and operational history. In some countries detailed information about the spent fuel assemblies can be retrieved from a dedicated management system, e.g. the Core Management System (CMSYS) developed at the Paul Scherrer Institut (PSI) [11][12]. Unfortunately, such a system is not always available making available information limited. To reduce the impact of limited information and identify possible errors in the fuel related input data, an experimental validation of the spent fuel properties is required. Therefore, two types of experimental data are important: data to assess and validate the performance of depletion codes and data to verify the design characteristics of the fuel and the operational history of the irradiated fuel. In this report basic principles of passive non-destructive assay (NDA) methods to characterise spent fuel are reviewed and the performance of available systems that can be applied under industrial conditions is discussed.

In the report, conventional uncertainty propagation based on normal distributions is applied. All uncertainties are standard uncertainties quoted at a 68 % confidence level and are given in standard compact notation. As much as possible the terminology of the International vocabulary of metrology – Basic and general associated terms are used [13].

2. Observables for non-destructive assay

Passive NDA relies on the detection of radiation emitted by the object of interest without the use of an external source to induce the emission. In this section the characteristics of radiation emitted by spent fuel is discussed, with a focus on radiation that can be used to characterise spent nuclear fuel samples, rods and assemblies by NDA without the need of a chemical treatment. This limits the discussion to decay heat, gamma-ray and neutron emission. The study is based on depletion calculations for UO_2 and MOX fuel applying irradiation conditions that are representative for a PWR. The weight fraction of the U and Pu isotopes in the fresh UO_2 and MOX fuel are specified in Table 1. The nuclide inventory is calculated using the Serpent code. Most of the results presented in this report are derived for a total burnup of 45 MWd/kg. Details about the fuel characteristics and irradiation conditions are given in [14].

Nuclide	Weight fraction	
	UO_2	MOX
^{234}U	0.00045	0.0000092
^{235}U	0.04794	0.0023
^{236}U	0.00001	0
^{238}U	0.95159	0.9176908
^{238}Pu	0	0.002
^{239}Pu	0	0.04376
^{240}Pu	0	0.02088
^{241}Pu	0	0.0076
^{242}Pu	0	0.00576

Table 1 – Weight fraction of U and Pu isotopes in the fresh UO_2 and MOX fuel used for the calculations reported in this report. The weight fractions are normalised to the total amount of U and Pu.

2.1 Decay heat

The decay heat rate or decay power density per unit volume emitted by spent fuel, which is denoted by p_r, can be calculated by:

$$p_r = \sum_i E_{ri}\, \lambda_i\, n_i \ , \tag{1}$$

where E_{ri} is the recoverable energy per decay, λ_i is the decay constant and n_i is the number of nuclei per unit volume or number density of the nuclide i. The recoverable energy per decay is the energy that is released due to the decay process and can be recovered as heat. The decay of a radionuclide by the emission of a charged particle, such as an α- or β-particle, usually leaves the daughter nucleus in an excited state. This results in the emission of γ-rays and/or conversion electrons. One usually assumes that the energy of the emitted charged particles and the secondary emission of γ-rays can be fully transferred into heat. Hence, in case of α-decay the recoverable energy E_{ri} is the total disintegration energy or *Q*-value. However, in case of β-decay a fraction of the disintegration energy is transferred into (anti)neutrino energy. This energy will not be converted into heat and the recoverable energy is determined by the energy distribution of the emitted γ-rays and electrons.

The decay power as a function of cooling time resulting from the irradiation of a fresh UO_2 and MOX fuel is presented in Figure 1. The contribution of α- and β-particles and γ-rays in case of irradiated UO_2 fuel is shown in Figure 2. The relative contribution of individual radionuclides is specified in Figure 3. The total decay heat rate for SNF originating from irradiated MOX fuel is larger compared to the one originating from irradiated UO_2 fuel. This is due to the contribution of the trans-uranium actinides (Pu, Am, Cm) when starting with MOX fuel. The largest contribution for cooling times between 1 a and 10 a, is due to relatively short-lived fission products chains, mainly ^{144}Ce/^{144}Pr and ^{106}Ru/^{106}Rh. The contribution of actinides for such cooling times is only significant in case of MOX fuel. For MOX fuel the contributions from ^{242}Cm and ^{244}Cm exceed 10%. For cooling times between 10 a and 30 a, contributions from the short-lived fission product chains become negligible. For UO_2 fuel, the decays of ^{90}Sr/^{90}Y and ^{137}Cs/^{137m}Ba have the largest contribution to the total decay heat. In case of MOX, the largest contribution is due to the decay of ^{244}Cm, followed by ^{238}Pu and ^{241}Am. With increasing cooling time the contribution from ^{241}Am becomes the dominant one. This is due to build-up of ^{241}Am by ^{241}Pu decay. Even though the relative contribution of the ^{137}Cs/^{137m}Ba decay is much smaller for MOX fuel, its absolute value is comparable to the one for UO_2 fuel. On the other hand, the contribution of the ^{90}Sr/^{90}Y decay is also smaller in absolute terms due to the lower cumulative yield of ^{90}Sr for neutron induced fission of ^{239}Pu and ^{241}Pu compared to the fission product yields for neutron induced fission of ^{235}U. For cooling times longer than 50 a, the decay heat for both SNF types is dominated by the contribution from the decay of ^{241}Am. Other contributions are due to the decay of ^{238,239,240}Pu. Contributions from light nuclides are getting smaller and eventually become negligible for cooling times longer than about 300 a.

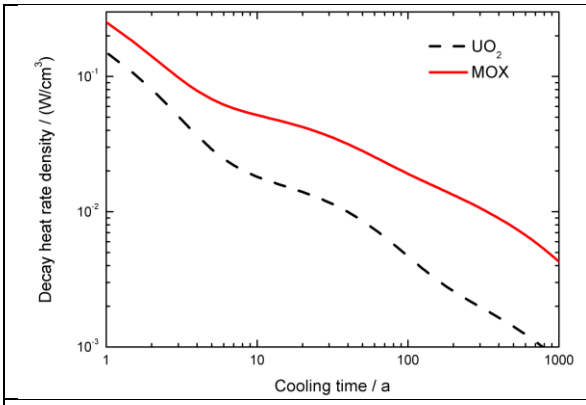

Figure 1 – Decay power density as a function of cooling time for a sample resulting from the irradiation of UO_2 and MOX fuel in a PWR up to a burnup of 45 MWd/kg.

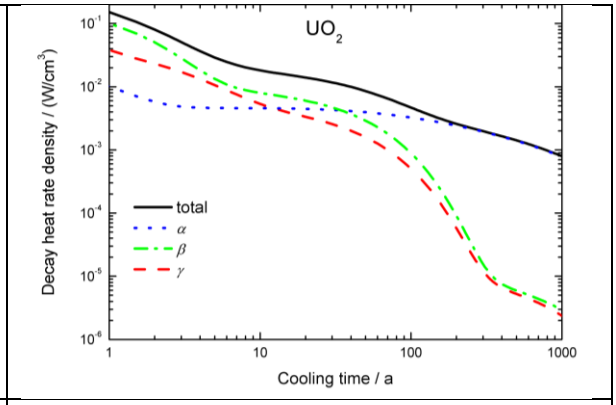

Figure 2 – Decay power density as a function of cooling time for UO_2 fuel irradiated up to a burnup of 45 MWd/kg. Contributions due to the emission of γ-rays and α- and β-particles are given.

Recommended decay data of key radionuclides contributing to the decay heat in spent fuel are reported in Table 2. These data, i.e. half-life and recoverable energy, are required for the calculation of the decay power. The data are taken from the Decay Data Evaluation Project (DDEP).

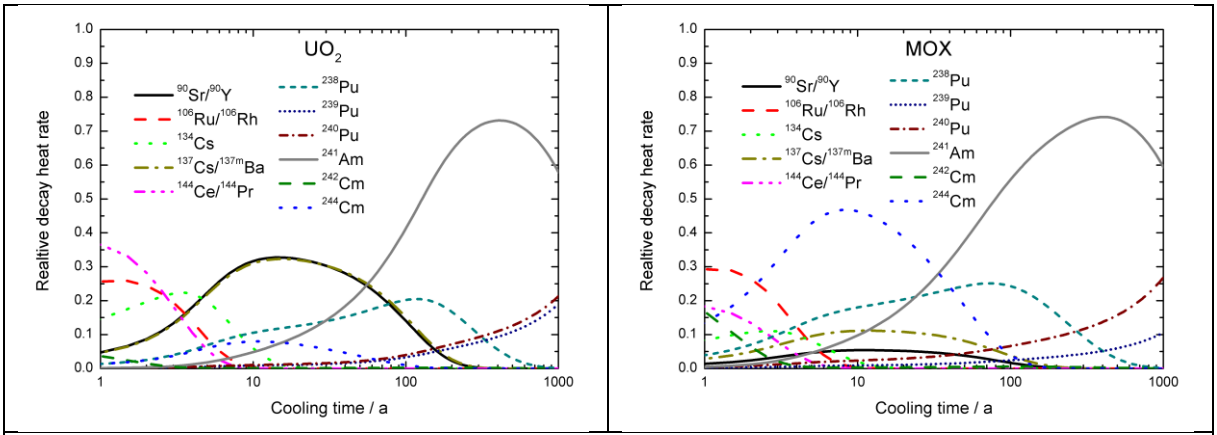

Figure 3 – Relative contribution of radionuclides to the total decay power as a function of cooling time. The spent fuel originates from the irradiation of UO_2 (left) and MOX (right) fuel in a PWR up to a burnup of 45 MWd/kg.

Nuclide	Half-life, $T_{1/2}$	$E_{r,\gamma}$ / keV	$E_{r,cp}$ / keV	E_r / keV
$^{90}Sr/^{90}Y$	28.8 (7) a / 2.6684 (13) d		1129.4 (14)	1129.4 (14)
$^{106}Ru/^{106}Rh$	371.5 (21) d / 30.1 (3) s	205.1 (15)	1424.4 (58)	1629.5 (60)
^{134}Cs	2.0644 (14) a	1554.7 (8)	163.8 (5)	1718.5 (9)
$^{137}Cs/^{137m}Ba$	30.05 (8) a / 2.552 (1) min	247.2 (12)	564 .6 (13)	811.8 (18)
$^{144}Ce/^{144}Pr$	284.89 (6) d / 17.29 (4) min	49.0 (6)	1286.4 (5)	1335.4 (7)
^{154}Eu	8.601 (4) a	1246.5 (48)	269.2 (38)	1515.7 (48)
^{238}Pu	87.74 (3) a		5593.20 (19)	5593.20 (19)
^{239}Pu	24100 (11) a		5224.51 (21)	5224.51 (21)
^{240}Pu	6561 (7) a		5255.75 (15)	5255.75 (15)
^{241}Am	432.6 (6) a		5637.82 (12)	5637.82 (12)
^{242}Cm	162.86 (8) d		6215.56 (8)	6215.56 (8)
^{244}Cm	18.11 (3) a		5901.74 (5)	5901.74 (5)

Table 2 – Decay data required to calculate the decay power produced by radionuclides present in spent fuel. The half-life ($T_{1/2}$) and recoverable γ-ray ($E_{r,\gamma}$) and total charged particle energy ($E_{r,cp}$) are given together with the total recoverable energy (E_r). Data are taken from DDEP [15].

2.2 Gamma-ray emission

As mentioned in section 2.1, gamma-rays are emitted during the decay process. The gamma-ray emission rate spectrum per unit volume, denoted by $s_\gamma(E)$, can be obtained from the nuclide inventory by:

$$s_\gamma(E) = \sum_{i,j} P_{\gamma ij}\,\delta(E - E_{\gamma ij})\,\lambda_i n_i \ , \tag{2}$$

where $P_{\gamma ij}$ is the emission probability of a photon with energy $E_{\gamma ij}$ per decay of the nuclide i and $\delta(x)$ is the Dirac delta distribution. The photon emission rate energy density $\varphi_{q\gamma}(E)$ is defined as:

$$\varphi_{q\gamma}(E) = s_\gamma(E)E \ . \tag{3}$$

The total γ-ray emission rate energy density becomes:

$$\Phi_{q\gamma} = \int_0^\infty s_\gamma(E)E\,dE \ . \tag{4}$$

The decay of fission products is the main contributor to the gamma-ray emission of spent nuclear fuel. Figure 4 shows the energy dependence of the γ-ray emission rate energy density $\varphi_{q\gamma}(E)$ for SNF originating from fresh UO_2 fuel. Only the contribution of γ-rays with an energy E_γ > 400 keV is presented. The total γ-ray emission rate energy density is plotted as a function of cooling time in Figure 5. For cooling times < 10 a, the γ-ray spectrum is dominated by γ-rays originating from the decay of relatively short-lived fission products, i.e. the decay of ^{95}Zr, ^{95}Nb, ^{106}Ru/^{106}Rh and ^{144}Ce/^{144}Pr. There is also a contribution of 511 keV γ-rays due to electron-positron annihilation following β^+ decays. For cooling times between 10 a and 30 a, the most prominent γ-rays originate from the decay of ^{134}Cs, ^{137}Cs/^{137m}Ba and ^{154}Eu. For cooling times between 30 a and 200 a, the 661 keV γ-ray due to the ^{137}Cs/^{137m}Ba decay dominates. For cooling times > 400 a there is practically only a contribution of γ-rays with an energy < 400 keV due to the decay of ^{241}Am, as illustrated in Figure 5. They will be absorbed by the fuel and cannot be detected by a gamma-ray detector. However, they will contribute to the decay heat. The discussion of the data in Figure 4 and Figure 5 reveal that the γ-ray spectra for cooling times < 100 a are dominated by the decay of fission products. Therefore, γ-ray spectra emitted by spent fuel originating from MOX fuel are very similar as those from UO_2 fuel. Some differences occur due to differences in fission product yields for neutron induced fission of ^{235}U and ^{239,241}Pu.

Evidently, gamma-rays following the decay of activation products such as ^{60}Co due to their production within the cladding or structural materials will also contribute to the gamma-ray emission. For the main radionuclides of interest the half-life and γ-ray energies and emission probabilities of the most intense gamma-rays as recommended by DDEP [15] are given in Table 3.

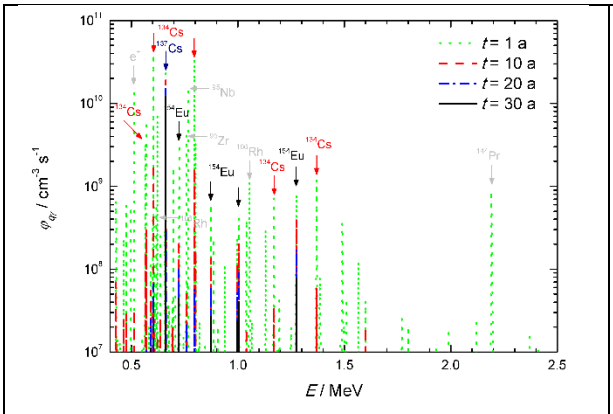

Figure 4 – Energy dependence of the γ-ray emission rate energy density $\varphi_{q\gamma}(E)$ by a fuel sample originating from the irradiation of UO_2 fuel in a PWR fuel up to a burnup of 45 MWd/kg.

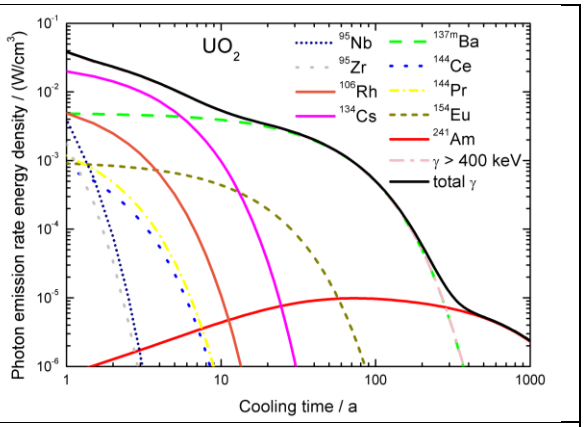

Figure 5 – Total γ-ray emission rate energy density and the contributions of some radionuclides as a function of cooling time of spent fuel originating from the irradiation of UO_2 in a PWR up to a burnup of 45 MWd/kg.

Nuclide	Half-life, $T_{1/2}$	E_γ / keV	I_γ
^{60}Co	5.2711 (8) a	1173.228 (3)	0.9985 (3)
		1332.492 (4)	0.999826 (6)
^{95}Zr	64.032 (6) d	724.193 (3)	0.4427 (22)
		756.729 (12)	0.5438 (22)
^{95}Nb	34.991 (6) d	765.803 (6)	0.99808 (7)
^{106}Ru / ^{106}Rh	371.5 (21) d / 30.1 (3) s	621.900 (40)	0.0987 (15)
		1050.390 (30)	0.01490 (25)
^{134}Cs	2.0644 (14) a	563.246 (3)	0.08342 (15)
		569.330 (2)	0.15368 21)
		604.720 (3)	0.9763 (8)
		795.860 (10)	0.8547 (9)
		801.950 (6)	0.08694 (16)
^{137}Cs / ^{137m}Ba	30.05 (8) a / 2.552 (1) min	661.657 (3)	0.8501 (20)
^{144}Ce / ^{144}Pr	284.89 (6) d / 17.29 (4) min	696.505 (4)	0.0141 (7)
		1489.148 (3)	0.00286 (3)
		2185.645 (5)	0.0073 (1)
^{154}Eu	8.601 (4) a	123.0706 (9)	0.4040 (50)
		723.3014 (22)	0.2005 (21)
		873.1834 (23)	0.1217 (12)
		1274.429 (4)	0.3490 (30)

Table 3 – Half-life ($T_{1/2}$) and γ-ray energy (E_γ) and number of γ-rays per decay (I_γ) of the most intense γ-rays for strong γ-ray emitting radionuclides in spent fuel. All mentioned nuclides are fission products, except ^{60}Co that is produced by neutron activation of Co impurities in the fuel, cladding and structural materials of the fuel assemblies. Data are taken from DDEP [15].

2.3 Neutron emission

The total neutron emission rate density s_n is the sum of contributions due to spontaneous fission (SF) and (α,n) reactions:

$$s_n = \sum_i (s_{SF,i} + s_{\alpha,i})\, n_i \ . \tag{5}$$

The specific neutron emission rate per nucleus due to SF and (α,n) reactions following the decay of nuclide i are denoted by $s_{SF,i}$ and $s_{\alpha,i}$, respectively. The specific SF neutron emission rate is given by:

$$s_{SF,i} = \langle \nu \rangle_i \lambda_{SF,i} \ , \tag{6}$$

where $\langle \nu \rangle_i$ is the average total number of neutrons emitted per SF and $\lambda_{SF,i}$ is the decay constant for SF of the nuclide i. The production of neutrons by (α,n) reactions is mostly treated under the assumption of an infinitely thick target, i.e. the thickness is sufficient to stop α-particles. The specific neutron emission rate due to α-decay of nuclide i becomes:

$$s_{\alpha,i} = \lambda_{\alpha,i} \sum_l \sum_k P(E_{\alpha k}) Y_l(E_{\alpha k}) \ , \tag{7}$$

where $\lambda_{\alpha,i}$ is the decay constant for α-decay of nuclide i, $P(E_{\alpha k})$ the probability that an α-particle is emitted with an energy $E_{\alpha k}$ by nuclide *i* and $Y_l(E_{\alpha k})$ is the neutron yield for an α-particle with an energy $E_{\alpha k}$. The latter is the number of neutrons produced per incident α-particle interacting with a material with number density n_l. The neutron yield Y_l can be expressed as:

$$Y_l(E_\alpha) = n_l \int_0^{E_\alpha} \frac{\sigma_l(\alpha,n)}{\left|\frac{dE}{dx}\right|} dE_\alpha \ , \tag{8}$$

where $\sigma_l(\alpha, n)$ is the neutron production cross section for target nucleus l and dE/dx is the linear stopping power of the target material.

Neutron emission by spent fuel is predominantly due to spontaneous fission of heavy nuclides, in particular ^{242}Cm and ^{244}Cm, and (α,n) reactions due to the presence of oxygen. The total neutron emission rate together with the contributions due to SF and (α,n) reactions as a function of cooling time are shown in Figure 6. The neutron emission rate originating from irradiated MOX fuel is about one order of magnitude larger compared to the one from irradiated UO_2 fuel. For irradiated MOX fuel SF neutrons are the dominating neutron source even for long cooling times. For irradiated UO_2 fuel the neutron production for cooling times <100 a is fully dominated by SF neutrons. For cooling times between 100 a and 500 a there is a relatively strong contribution from neutrons produced by (α,n) reactions.

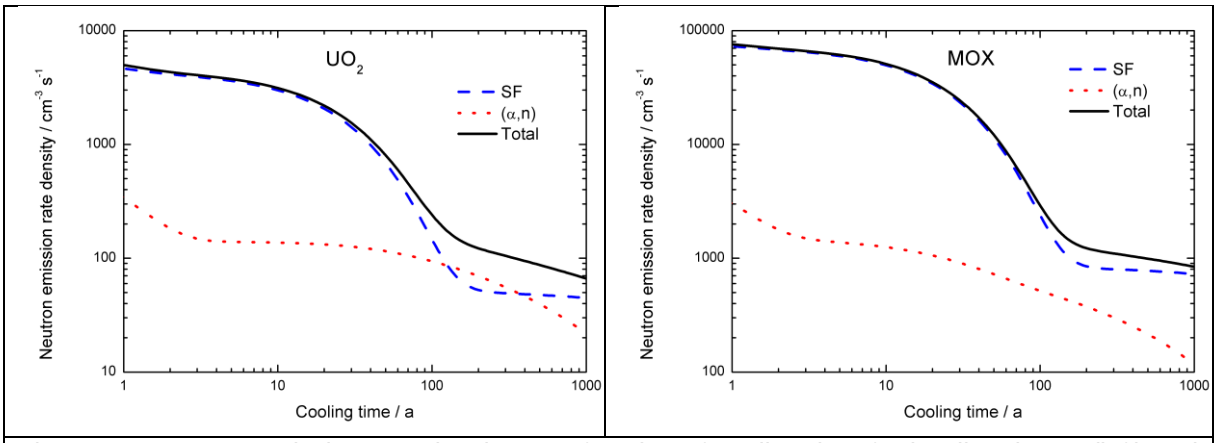

Figure 6 – Neutron emission rate density as a function of cooling time for irradiated UO_2 (left) and MOX (right) fuel. The irradiation is in a PWR to a total burnup of 45 MWd/kg. The contribution due to SF and (α,n) neutrons is shown.

Figure 7 shows the relative contribution of specific radionuclides to the neutron emission originating from spontaneous fission as a function of cooling time. Due to its relatively short half-life, i.e. $T_{1/2}$ = 0.446 a, ^{242}Cm is only important for short cooling times. The dominant contributor to the SF neutron emission rate for cooling times up to about 100 a is ^{244}Cm. For cooling times between 100 a and 1000 a, the most important contributor is ^{246}Cm, followed by ^{240}Pu and ^{242}Pu. For irradiated MOX fuel, the contribution of ^{246}Cm relative to ^{240,242}Pu is higher compared to the its contribution in irradiated UO_2 fuel, due to the much higher build-up of ^{246}Cm.

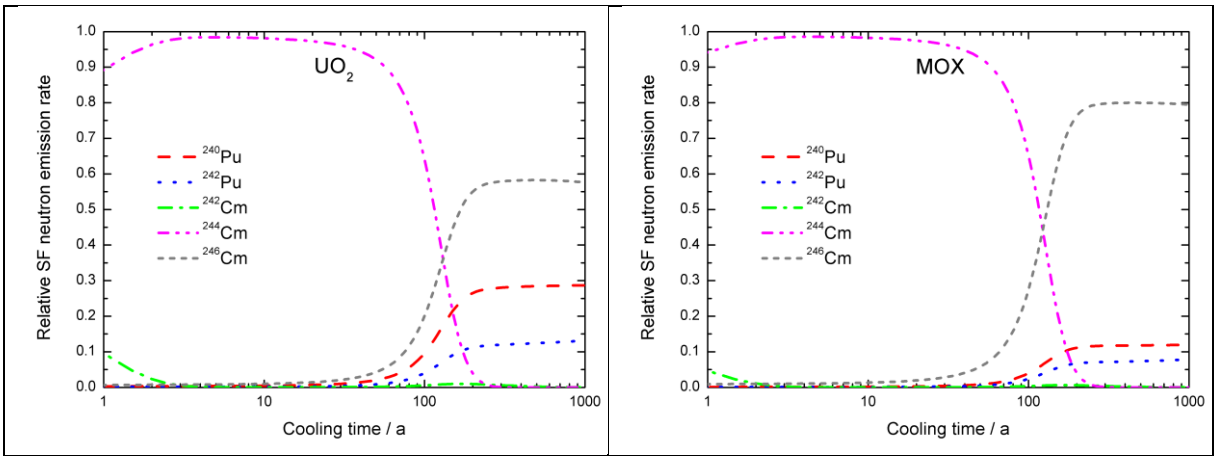

Figure 7 – Relative contribution to the total number of spontaneous fission neutrons emitted by ^{240,242}Pu and ^{242,244,246}Cm as a function of cooling time. The results are shown for irradiated UO_2 (left) and MOX (right) fuel. The irradiation is in a PWR to a total burnup of 45 MWd/kg.

The contributions to the neutron emission rate by (α,n) reactions are mainly due to the α-decay of ^{238,239,240}Pu, ^{241}Am and ^{242,244}Cm. Their relative contributions to the neutron emission by (α,n) reactions are plotted as a function of cooling time in Figure 8. The contribution of ^{242}Cm to the neutron emission by (α,n) reactions is only important for short cooling times when the total (α,n) contribution to the total emission rate is very small. For cooling times between 2 a and 30 a, the most important contribution to the (α,n) neutrons comes from the α-decay of ^{238}Pu and ^{240}Pu followed by the decay of ^{241}Am. For even longer cooling time the relative contribution of ^{241}Am increases. For cooling times > 300 a, contributions from ^{239,240}Pu become relatively more important.

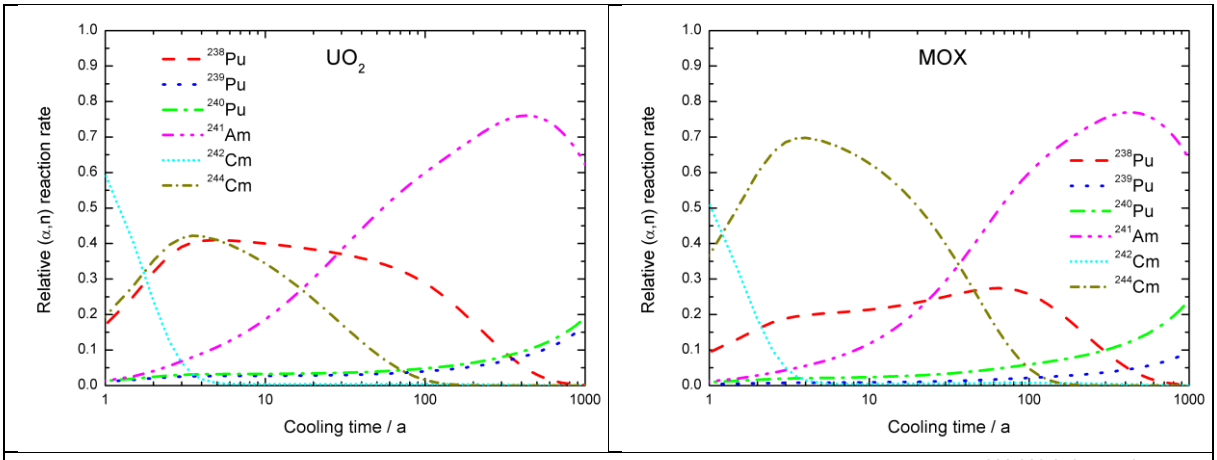

Figure 8 – Relative contribution to the total number of (α,n) neutrons emitted by ^{238,239,240}Pu, ^{241}Am and ^{242,244}Cm as a function of cooling time. The results are shown for irradiated UO_2 (left) and MOX (right) fuel. The irradiation is in a PWR to a total burnup of 45 MWd/kg.

Nuclear data needed to calculate the emission rate of spontaneous fission neutrons and neutrons produced by (α,n) reactions in spent fuel are specified in Table 4. The half-life and the branching fraction for spontaneous fission are taken from DDEP [15]. The average number of prompt fission neutrons are from the evaluation of Santi and Miller [16]. The specific neutron production rate per mass of nuclide by (α,n) reactions in UO_2 (Y_α) were obtained with the SOURCES code [17][18].

Nuclide	Half-life, $T_{1/2}$	β_{sf}	$<\nu>$	Y_α / (s^{-1} g^{-1})
^{238}Pu	87.74 (3) a	1.85 (5) 10^{-7}	2.190 (70)	1.63 10^{4}
^{239}Pu	24100 (11) a			4.52 10^{1}
^{240}Pu	6561 (7) a	5.70 (20) 10^{-8}	2.154 (5)	1.72 10^{3}
^{242}Pu	3.73 (3) 10^{5} a	5.50 (9) 10^{-6}	2.149 (8)	
^{241}Am	432.6 (6) a			3.29 10^{3}
^{242}Cm	162.86 (8) d	6.36 (14) 10^{-8}	2.540 (20)	4.45 10^{6}
^{244}Cm	18.11 (3) a	1.36 (1) 10^{-6}	2.710 (10)	9.23 10^{4}
^{246}Cm	4723 (27) a	2.615 (7) 10^{-4}	2.930 (30)	

Table 4 – Data required to calculate the neutron emission rate by spent nuclear fuel. The half-life ($T_{1/2}$) and the branching fraction for spontaneous fission (β_{sf}) are taken from DDEP [15]. The average number of prompt fission neutrons ($<\nu>$) are from the evaluation of Santi and Miller [16]. The specific neutron production neutron emission rate per mass of nuclide by (α,n) reactions in UO_2 (Y_α) are obtained with the sources code [17][18].

For the development of an NDA system that relies on the detection of neutrons emitted by irradiated fuel the energy distribution of the emitted neutrons is important. The distribution for prompt fission neutrons following spontaneous fission of ^{244}Cm and (α,n) neutrons produced in the fuel are compared in Figure 9. The experimental data reported by Boykov et al. [19] are compared with distributions resulting from a parameterisation using a Maxwellian and Watt distribution. The parameters for the parameterisation, which are given in Table 5, were derived from a fit to the data of Boykov et al. [19]. The energy distribution of (α, n) neutrons was parameterised by an analytical function proposed in [20], with the parameters specified in Table 5. The result of the analytical expression is compared with the spectrum for (α, n) neutrons calculated with the SOURCES 4C code developed at LANL.

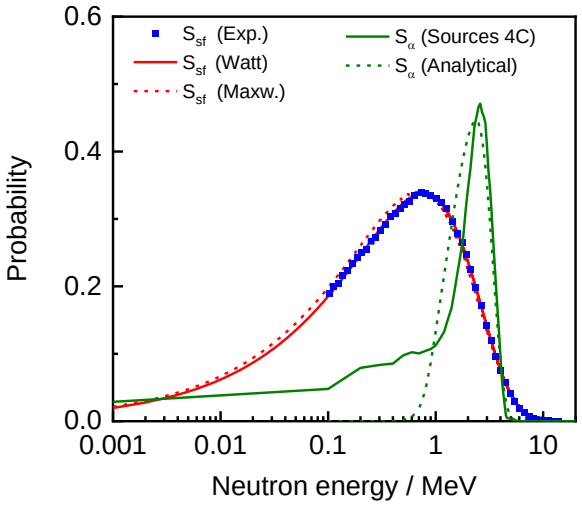

Figure 9 – Energy distribution of prompt fission neutrons from ^{244}Cm(sf) and (α, n) neutrons produced in spent fuel. For ^{244}Cm(sf) the experimental distribution of Boykov et al. [19] is compared with the results of a parameterisation using a Watt and Maxwellian distribution. The analytical expression for the distribution of (α, n) neutrons proposed in [20] is compared with results of calculations using the SOURCES code (version 4C) [17][18].

^{244}Cm(sf)	(α, n) in UO_2 spent fuel	
	Energy region	Distribution
Maxwellian ($kT = 1.39$ MeV)	$E < 0.8$ MeV	$0.2207(E/E_0)^{6.4}$ with $E_0 = 1$ MeV
Watt a = 0.620 MeV, b = 0.952 MeV	0.8 MeV $\leq E < 2.4$ MeV	$-0.3746 + 0.6448E/E_0 - 0.138(E/E_0)^2$
	$E \geq 2.4$ MeV	$0.3803 \exp[-0.77\ (E/E_0 - 2.31)^2]$

Table 5 –Parameters for a parameterisation of the energy distribution of prompt fission neutrons from ^{244}Cm(sf) by a Maxwellian and Watt distribution. The parameters are derived from a fit to the data of Boykov et al. [19]. The analytical expression describing the energy distribution of neutrons produced by (α, n) in spent UO_2 fuel is taken from [20].

2.4 Key radionuclides for NDA of spent fuel

From the discussion in Section 2 radionuclides that are important for the characterisation of spent nuclear fuel by NDA are identified and listed in Table 6. The table includes the half-life and the observable of interest for NDA of spent fuel. Evidently, these nuclides are also important to evaluate the neutron and gamma-ray emission properties of spent fuel assemblies as part of any safety analysis for transport, storage and disposal of spent fuel [21][22].

Radionuclide	Half-life, $T_{1/2}$	decay heat	neutron emission	γ-ray emission
^{60}Co	5.2711 (8) a			x
^{90}Sr/^{90}Y	28.8 (7) a / 2.6684 (13) d	x		
^{95}Zr	64.032 (6) d			x
^{95}Nb	34.991 (6) d			x
^{106}Ru / ^{106}Rh	371.5 (21) d / 30.1 (3) s	x		x
^{134}Cs	2.0644 (14) a	x		x
^{137}Cs / ^{137m}Ba	30.05 (8) a / 2.552 (1) min	x		x
^{144}Ce / ^{144}Pr	284.89 (6) d / 17.29 (4) min	x		x
^{154}Eu	8.601 (4) a	x		x
^{238}Pu	87.74 (3) a	x	x	
^{239}Pu	24100 (11) a	x		
^{240}Pu	6561 (7) a	x		
^{242}Pu	3.73 (3) 10^5 a			
^{241}Am	432.6 (6) a	x	x	
^{242}Cm	162.86 (8) d	x	x	
^{244}Cm	18.11 (3) a	x	x	
^{246}Cm	4723 (27) a		x	

Table 6 – Radionuclides that have a substantial contribution to the decay heat, gamma-ray and neutron emission by spent fuel. The half-life ($T_{1/2}$) is taken from DDEP [15].

3. NDA measurements for code validation

At present the validation of depletion codes strongly relies on nuclide inventory data that result from destructive chemical and radiochemical analysis of spent fuel rod segments, also referred to as Post Irradiation Examination (PIE) [23][24]. Experimental data resulting from NDA that is used to validate depletion codes is rather scarce. In this paragraph NDA methods that can be used to validate codes are discussed. The discussion includes results of improved analysis procedures for the calorimeter installed at Clab and an innovative method to characterise a spent fuel segment sample, both resulting from activities performed within Task 2 of WP8.

3.1 Rod scanning by gamma-spectrometry

Every PIE starts with a selection of representative segment samples used for further destructive chemical and radiochemical analysis. The selection of a representative sample is mostly performed by gamma-ray spectroscopic scanning measurements of the fuel rod to determine the axial activity distribution of specific radionuclides such as ^{134,137}Cs and ^{154}Eu. The system consists of a gamma-ray detector, mostly a High Purity Germanium (HPGe) detector, with a gamma-ray collimation system placed between the rod and the detector. Gamma-rays emitted by the spent fuel rod pass through the slit of the collimator. The dimensions of the collimator are optimised with respect to the required spatial resolution. Based on the results of a rod scan the positions of the fuel pellets can be identified and a proper sampling strategy can be defined [23] [26]. When aiming for a complete inventory analysis, the inhomogeneity of the spent fuel has to be taken into account. Therefore, a large enough sample should be taken that includes pellets as well as pellet gaps by cutting from mid-pellet to mid-pellet, including that way a full inter-pellet area. The corresponding equivalent of one full pellet is the minimum sample size for a complete inventory analysis, though two or three pellets (thus including two or three inter-pellet areas) might even be preferred.

An example of such a gamma-ray scanning profile is shown in Figure 10. This profile was obtained at the Laboratory for High and Medium level Activity (LHMA) of SCK CEN (BE). The measurements were carried out to determine the burnup profile of the fuel rod D05, which was taken from a 15 × 15 assembly that was irradiated in the Tihange 1 PWR. The study of this rod is part of the Rod-Extremity and Gadolinia AnaLysis (REGAL) program coordinated by the SCK CEN [27]. Details of the fuel composition and geometry and irradiation history are given in [28].

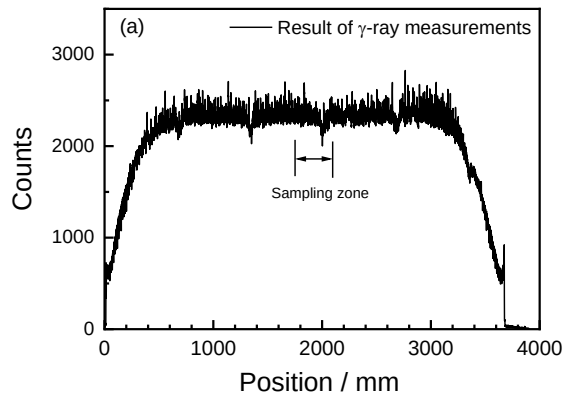

Figure 10 – Results of a gamma-ray scanning measurement of the D05 fuel rod performed at the LHMA facility of SCK CEN. The axial positions are relative to the bottom end of the fuel rod.

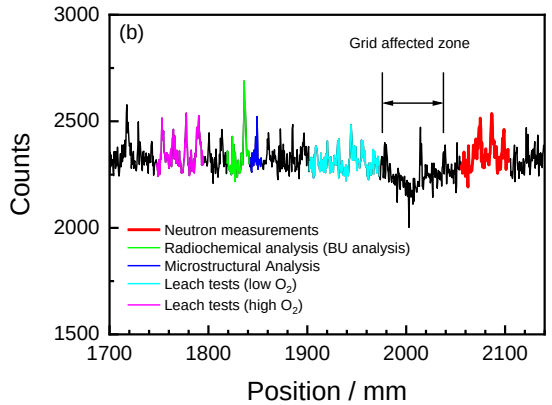

Figure 11 – Results of the scanning measurements in the sampling zone between 1700 mm and 2150 mm. Samples taken for different investigations are indicated with colours.

The regular peaking pattern observed in the high burnup region of the rod, between 750 mm and 3250 mm, is due to local migration of Cs to the pellet-pellet interfaces. Grid positions are clearly distinguished every 700 mm. The D05 rod was used to select samples taken for different types of investigations. The sampling in the axial region between 1750 mm and 2100 mm is represented in Figure 11. Leaching samples were used to investigate instant release of fission products under repository conditions [29] [30]. The results of microstructural analyses using a sample that was taken from the region between 1843 mm and 1854 mm are reported in [31]. A sample to determine the nuclide inventory by radiochemical analysis was taken from the region between 1819 mm and 1842 mm. The results included the inventory of ^{137}Cs, $^{143+144}$Nd, $^{145+146}$Nd, ^{148}Nd and ^{150}Nd to be used as burnup indicators [27].

A sample, taken from the region between 2056 mm and 2104 mm, was used to develop and demonstrate within WP8 an absolute NDA method to determine the neutron production rate of a spent fuel segment sample [32] [33]. The average count rates resulting from the gamma-ray scan for the sample for the neutron measurements (red) was 2337 (7) s^{-1} and for the sample that was analysed by radiochemical analysis (green) was 2341 (14) s^{-1}. The difference of 0.17% is a factor 3 less than the combined uncertainty due to counting statistics. The characteristics of the segment sample are given in Table 7. The main uncertainty of the net weight of the fuel material is due to the uncertainty on the state of the cladding material: uncertainty of the wall thickness, degree of oxidation and presence of deposits. Details about the neutron measurements are given in section 3.2.

Parameter	
Length	52.01 (4) mm
Segment weight	42.616 (1) g
Cladding weight	6.71 (4) g
Net fuel weight	35.91 (4) g

Table 7 – Characteristics of the SNF segment sample that was used for the neutron measurements at the LHMA facilities of SCK CEN.

Similar rod scanning measurements were carried out to select representative samples for radiochemical analysis to study the performance of depletion codes [34]. The results of the scanning measurements were used to determine the burnup profile of a rod from which 8 samples were sampled. The samples were analysed by Inductively Coupled Plasma Mass Spectrometry (ICP-MS), including isotope dilution analysis, to determine the burnup and inventory of 60 nuclides covering 21 elements. The ICP-MS measurements were performed after separation by High Performance Liquid Chromatography (HPLC). These data were used within WP8 to verify the performance of CASMO5 and the Polaris module of SCALE [35].

3.2 Neutron emission measurements of a segment sample

An innovative NDA method was developed within WP8 to determine the neutron emission rate of a spent fuel segment sample avoiding any reference to a representative spent nuclear fuel sample to calibrate the detection system. Special procedures were defined to perform the measurements under standard controlled area conditions using a transportable neutron well counter that is routinely used for nuclear safeguards verification measurements. The procedures were adapted to the hot cell facility at the Laboratory for High and Medium level Activity (LHMA) of SCK CEN in Belgium. The procedure can be applied to any neutron counter that is optimised for neutron correlation measurements. The method and experimental and analysis procedures are described in [32][33].

The method relies on a transfer procedure that is adapted to the hot cell facilities at the LHMA facility of the SCK CEN (BE). A neutron correlation counter was used to separate the contribution of spontaneous fission and (α,n) neutrons. It is a transportable neutron well counter that is routinely used for nuclear safeguards verification measurements [36] [37]. The detector consists of 42 ^{3}He proportional counters embedded in polyethylene that is used as neutron moderator. The counters are divided into six groups. Each group is connected to one Amptek A-111 hybrid preamplifier, discriminator and pulse shaper board. The logic output of each board is sent to an OR gate. The output of this OR gate is used as an input for a JSR-12 shift register [38][39], which is used to register the total number of detected events and the number of events that are detected in two time windows that are opened (triggered) by each neutron detection event. The first window is opened a short time (or pre-delay) t_p = 4.5 μs after each trigger event. The accumulated content, referred to as 'Reals + Accidentals' or 'R+A', is due to a contribution of real coincident events and accidental coincident events. The second gate is opened at a very long time delay after the first gate. Its content provides a direct measure of the accidental coincident events. From the counts in these two windows the recorded totals and reals rate are derived, which are denoted by T and R, respectively.

Experiments with ^{252}Cf(sf) sources were carried out at JRC Ispra to determine the main characteristics of the detector: parameters for an empirical dead time correction, gate fraction and detection efficiency. The sources were certified for the neutron production rate and isotopic composition. The point model proposed by Hage and Cifarelli [40] was applied to determine the production rate of prompt fission neutrons from spontaneous fission and the α-ratio between the production rate of neutrons produced by (α,n) reactions. Assuming that all neutrons follow a similar energy distribution, the contribution due to delayed neutrons can be neglected and neutrons are only absorbed by neutron induced fission, the relation between the expected totals T and reals rate R and the sample properties are [40]:

$$T = \varepsilon S_{sf} M [1 + \alpha] \quad . \tag{9}$$

$$R = \varepsilon^2 f S_{sf} M^2 \left[\frac{\nu_{sf(2)}}{\nu_{sf(1)}} + \frac{p \nu_{(2)}}{1 - p \nu_{(1)}} (1 + \alpha)\right]. \tag{10}$$

with:

- S_{sf} is the production rate of spontaneous fission neutrons in the sample,
- α is the ratio of the production rate of spontaneous fission neutrons and neutrons produced by (α,n) reactions in the sample,
- the detection efficiency for a fission neutron,
- f the gate fraction,
- M the neutron multiplication,
- p the probability to produce a neutron induced fission event by a fission neutron,
- $\nu_{sf(1)}$ and $\nu_{sf(2)}$ the first and second order normalised factorial moments of the neutron multiplicity distribution for prompt fission neutrons from spontaneous fission,
- $\nu_{(1)}$ and $\nu_{(2)}$ the first and second order normalised factorial moments of the neutron multiplicity distribution for neutron induced fission by prompt fission neutrons from induced fission.

For the analysis a multiplication of M = 1.006 was assumed. This multiplication, which was derived by Monte Carlo simulations [41], is consistent with the one derived in [42].

Measurements to determine the neutron production rate of a spent fuel segment were performed at the LHMA facility. The procedure to prepare the sample together with its characteristics were discussed in section 3.1. The neutron production rate of this REGAL sample due to spontaneous fission derived from the measurements is S_{sf} = 680 (15) $s^{-1}g^{-1}$. A detailed uncertainty evaluation was performed and the results are summarised in Table 8. This table specifies the contribution of the uncertainty due to the counting statistics, detection efficiency, gate fraction, first and second order factorial moments for ^{244}Cm(sf) and multiplicity. The main contribution of the uncertainty of the spontaneous fission rate is due to the second order factorial moment, detection efficiency and gate fraction. The α-ratio α = 0.035 (18) is determined with an uncertainty of about 50%. Therefore, this value cannot be used to validate codes. The uncertainties of the neutron production rate from spontaneous fission and α-ratio can be reduced by optimising the detector design, i.e. increase detection efficiency, reduce dead time, improve the die-away time, and by reducing the uncertainty on the nuclear data, in particular the one of the second order factorial moment.

Uncertainty component, x_j	$\frac{u_{x_j}}{x_j}$	$\frac{u_{S_{sf},j}}{u_{S_{sf}}}$	$\frac{u_{\alpha,j}}{u_{\alpha}}$
Totals rate, T	0.0008	< 0.01	0.05
Reals rate, R	0.0027	0.15	0.17
Detection efficiency, ε_{sf}	0.0055	0.60	0.35
Gate fraction, f	0.0071	0.40	0.45
First order factorial moment, $\nu_{sf(1)}$	0.0037	0.20	0.25
Second order factorial moment, $\nu_{sf(1)}$	0.0120	0.67	0.80
Multiplication, M	0.0020	0.01	< 0.01

Table 8 – Contribution of the counting statistics, the detection efficiency, gate fraction, first and second order factorial moments for ^{244}Cm(sf) and neutron multiplication to the uncertainty of the derived neutron production rate due to spontaneous fission and the α-ratio.

The value derived from the direct neutron measurements is within uncertainties in agreement with the one derived from the nuclide inventory of the adjacent sample, which is S_{sf} = 699 (28) $s^{-1}g^{-1}$. This results in a weighted average of S_{sf} = 684 (11) $s^{-1}g^{-1}$. Note that the uncertainty of the direct neutron measurement is more than a factor 2 smaller. Hence, this NDA method is a valuable radiometric method to complement radiochemical analysis techniques for depletion code validation. It does not require chemical treatments such as dissolution of the spent fuel sample including the cladding and further dilution and/or chemical separation processes. Evidently, this reduces the impact of systematic effects due to sample preparation and allows for the production of a reference sample that is not lost due to chemical processes. The results of the neutron emission rate measurements with the REGAL sample together with the data book, containing the design properties and irradiation history of the assembly, were used within WP8 to assess the performance of ALEPH2 [2], the TRITON/KENO-V.a module of SCALE [10] and Serpent 2 [7][8]. The results of that study are part of the EURAD deliverable 8.6 and are reported in [33].

After the successful completion of the first campaign an optimised detection system was designed and constructed. It will be used for new measurements of the same sample at LHMA to reduce the uncertainty of the neutron emission rate of the REGAL sample. The new system opens up for the possibility to measure high neutron emitting samples from irradiated MOX fuel and samples with a low neutron emission rate and relatively high γ-ray emission rate, such as the segments from the bottom and top part of a fuel rod. Unfortunately, these measurements will start after the end of the EURAD project.

3.3 Decay heat measurements of spent fuel assemblies at Clab

Calorimetry is a method that can be applied to determine the decay heat that is produced by spent fuel [43][44][45][46]. At present the only calorimeter in operation to determine the decay heat rate of a spent nuclear fuel assembly is installed at the Clab facility in Sweden [46][47]. The design of the calorimeter, shown in Figure 12, is based on the one that was used at GE Morris Operations [48]. It can accommodate BWR and PWR-types of assemblies. The device is about 4.9 m long with an external diameter of 0.45 m. The inner cylinder with an inner diameter of 0.33 m is used as the measurement chamber. A fixed insert is installed to keep the PWR assemblies centered and vertical. To place and center BWR assemblies and the electrical heater a removable insert is used.

This calorimeter is extensively used to validate the potential of depletion codes to predict the decay power of irradiated assemblies [49][50][51][52][53][54][55][56][57][58]. To improve the use of the data produced by the Clab calorimeter, a detailed study of the measurement principle of the calorimeter was performed within WP8. Optimised analysis procedures were defined. The procedures including a include criteria to select high quality experimental data and a statistical analysis to assess the measurement uncertainties and derive realistic confidence limits. A paper describing the full details of this study including a full uncertainty evaluation is in progress. The main results are discussed in this report. The design of the calorimeter is schematically represented in Figure 12.

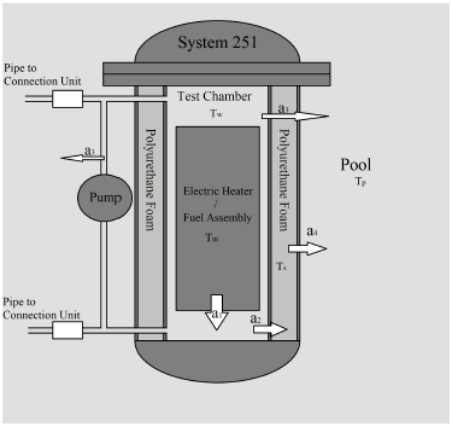

Figure 12 – Schematic representation of the calorimeter that is installed at the Clab facility.

The calorimeter at Clab is a semi-isothermal heat conduction calorimeter. The heat released within the vessel or measurement chamber flows to the pool. The pool, which is supposed to be at a constant temperature, acts as a surrounding heat sink. The temperature increase method is applied to establish the decay power of a spent fuel assembly. After the assembly or electrical heater is placed in the calorimeter, the lid is closed. To ensure that the calorimeter is completely filled with water, water is pumped into the calorimeter with the measurement flow pump until water flows out of the outlet. Deionised water is pumped into the calorimeter to bring the temperature of the water in the calorimeter below the pool temperature. Once the water in the calorimeter is well below the temperature of the pool water circulation of cooling water is stopped and the temperature will start to increase. The centrifugal circulation pump is started to maintain a homogeneous temperature within the calorimeter. The temperature sensors installed at different locations in the measurement chamber and the pool are recorded at regular time intervals.

The difference of the temperature in the measurement chamber and the pool (ΔT) is determined as a function of time. The gradient of the temperature increase as a function of time is used to derive the thermal power produced in the calorimeter. The gradient is calculated at the time that the temperature difference between the measurement chamber and the pool is zero, i.e. $\Delta T = 0$. The gradient is determined by parameterising the temperature difference with an analytical function. The parameters of this function are derived by a fit to the data. An example of such a parameterisation to determine the temperature gradient $G = d\Delta T/dt$ at the time for which $\Delta T = 0$ is shown in Figure 13. The translation of

the rate of temperature increase to decay power is based on calibration measurements using an electrical heater, which simulates an irradiated fuel assembly. An example of such a calibration curve based on a linear relationship between the gradient and power of the electrical heater is shown in Figure 14. Once this calibration curve is established, the temperature gradient measured with an assembly in the calorimeter can be translated into a measured decay power (P_m). To derive the full recoverable energy or decay power (P) produced by a spent fuel assembly from the measured decay power, two corrections are required: a correction factor (K) for the difference in heat transfer properties between measurements with the electrical heater and the assembly and a correction (P_e) for the heat loss due to gamma-rays escaping from the calorimeter. The full decay power produced by the assembly becomes:

$$P = P_e + K\,P_m, \tag{11}.$$

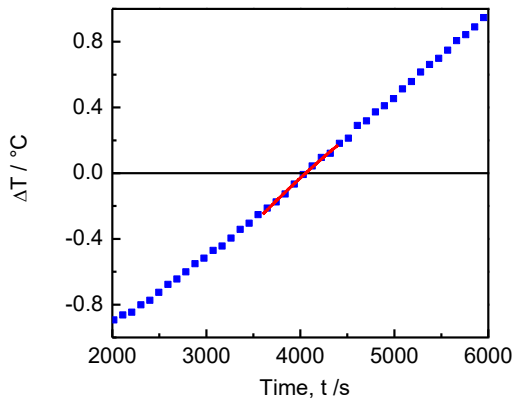

Figure 13 – Difference between the temperature of the water in the calorimeter and in the pool as a function of time. The line in red is a polynomial fit to the data to derive the gradient G = dΔT/dt at the time that ΔT = 0.

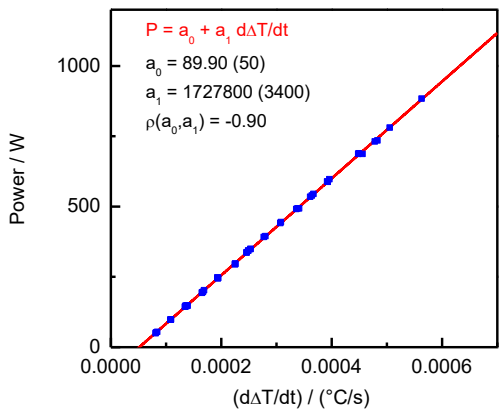

Figure 14 – The power delivered by the electrical heater as a function of the temperature gradient derived from the temperature difference measurements. The red line is the result of a fit to the data using a linear relation.

To derive the correction factor to account for the difference in heat transfer properties between the electrical heater and assembly it is assumed that the electrical heater or assembly, the water in the measurement chamber and the structure of the calorimeter are in thermal equilibrium. Under these conditions a one component heat transfer model can be applied and the relation between the temperature gradient and heat rate production within the measurement chamber becomes [59][60]:

$$P_m = C\left(\frac{d\Delta T}{dt}\right) + k\,\Delta T, \tag{12},$$

with P_m the power generated in the calorimeter, C the heat capacity of the material of the calorimeter that is in thermal equilibrium, ΔT the difference in temperature in the calorimeter and the pool and k the thermal conductivity between the calorimeter and the pool. Since the gradient G = dΔT/dt is derived at the time that the temperature difference is zero, i.e. ΔT = 0, the relation becomes:

$$P_m = C\left(\frac{d\Delta T}{dt}\right) \tag{13}.$$

Based on this model the correction factor K in Eq. 11 is the ratio between the heat capacity with the fuel assembly in the calorimeter and the one with the electrical heater in the calorimeter. Since the total heat capacity in the calorimeter is dominated by the water, this correction factor is mainly determined by the ratio of the water volume with an assembly and with the heater present in the calorimeter. An evaluation for this correction factor together with its uncertainty is reported in the R-05-62 report of Clab [46]. The correction factors for BWR and PWR assemblies that are stored at Clab are about $K_{BWR} \approx 0.964$ and $K_{PWR} \approx 0.915$, respectively, with an uncertainty of about 0.7%. This uncertainty is derived based on a conservative 10% uncertainty of the assembly volume [46].

Part of the gamma-rays emitted by spent fuel assemblies will escape from the calorimeter into the pool without depositing their energy in the calorimeter. Therefore, a fraction of the recoverable energy will not contribute to the measured power. In report R-05-62 this fraction is derived from measurements with gamma-ray dosimeters placed outside the calorimeter combined with analytical expressions establishing a relation between the escape power and the results of the dose-rate measurements. Within WP8 a different approach based on gamma-ray transport calculations was defined. In a first step, the energy of a mono-energetic gamma-ray that escapes from the calorimeter is calculated, supposing that this gamma-ray originates from a radionuclide that is homogeneously distributed in the assembly. This results in a correction factor as a function of gamma-ray energy. The correction factors for PWR assemblies measured at Clab are shown in Figure 15. In the second step, the nuclide inventory is calculated using a depletion code and the gamma-ray emission spectrum is derived based on the gamma-ray emission probabilities recommended by DDEP and the contribution of Bremsstrahlung. The latter is derived using the energy distribution of electrons in DDEP as an input to MCNP. The final correction is obtained by applying the correction factor as a function of gamma-ray energy to the gamma-ray emission spectrum derived from the depletion calculations. For the data presented in this report the gamma-ray transport and depletion calculations were both derived from calculations with Serpent.

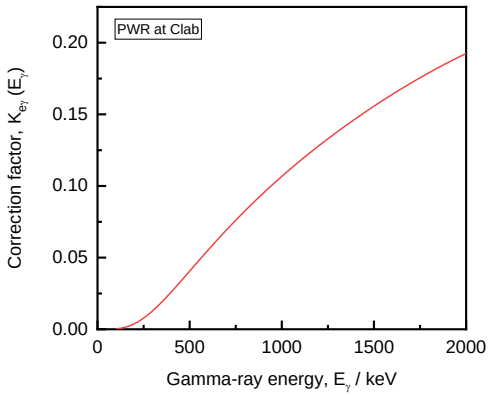

Figure 15 – Correction factor as a function of gamma-ray energy to account for energy that is lost due to gamma-rays escaping from the calorimeter. The correction factor is for PWR assemblies stored at Clab and is obtained by gamma-ray transport calculations with Serpent.

In parallel to the work done within WP8, SKB and Vattenfall AB as part of an Electric Power Research Institute (EPRI) project performed a fully independent study. The two independent procedures were used to re-analyse the results of the calorimetric measurements reported by Jansson et al. [58]. In **Erreur ! Source du renvoi introuvable.** the decay heat rate together with the correction for gamma-rays heat loss derived by the two independent procedures are compared with those of [58]. This comparison reveals that the independent procedures from EURAD and EPRI produce fully consistent results. However, they suggest that the results of Jansson et al. [58] suffer from a systematic error and are overestimated by about 2%. The analysis procedures defined within the EURAD and EPRI projects were applied to derive the decay power of PWR and BWR assemblies which were part of the SKB-50 campaign. The results of these data were used to prepare the deliverable 8.6.

In addition, all calibration data performed at Clab were reviewed applying the procedures developed within WP8. This review revealed that the calibration applied in the R-05-62 report [46] could introduce a systematic error. The procedure in the R-05-62 report [46] uses two different calibration curves for decay power below 350 W and for a decay power between 250 W and 950 W. The review demonstrates that such a separation is not justified and is not consistent with the measurement method and principle, in particular the assumptions made to apply Eqs. 12 and 13. Unfortunately, the results of PWR and BWR fuel measurements were not available in time to verify the impact of the difference in calibration of the assembly data before the end of the EURAD project. Based on these findings and the extensive use of the calorimetric data of the Clab calorimeter for code validation, it is recommended that the results of the measurements reported in the R-05-62 report [46] are revised using the procedures obtained within

the EURAD project. The results of such an analysis is in progress and will be included in the paper that is in preparation. It is expected that the results of this study will strengthen the idea to include calorimetric data into the SFCOMPO database [24].

ID	Jansson et al.[58]			WP8 – EURAD			SKB/Vattenfall - EPRI		
	P_e / W	P_m / W	P / W	P_e / W	P_m / W	P / W	P_e / W	P_m / W	P / W
BT01	58	1546	1604	49.4	1535	1584	49.2	1531	1580
BT02	30	1008	1038	25.3	998	1023	24.7	994	1019
BT03	21	853	874	20.6	839	860	20.3	837	857
BT04	15	738	753	15.0	726	741	13.8	725	739
BT05	12	639	651	12.8	627	640	11.5	628	639

Table 9 – Decay powers (P, P_m and P_e) resulting from measurements at the Clab facility reported in [58]. Results of an independent analysis within WP8 and EPRI are compared with the original data reported by Jansson et al. [58].

4. NDA measurements to verify assembly characteristics

Most of the NDA systems used for the characterisation of spent fuel assemblies have been developed to verify the amount of fissile material for nuclear safeguards applications [61][62][63] or to verify the burnup for nuclear criticality safety applications applying a BurnUp Credit (BUC) approach [64][65][66]. The Next Generation Safeguards Initiative – Spent Fuel (NGSI−SF) established by the Department Of Energy (DOE) of the United States of America triggered the development and testing of new NDA techniques to characterise spent nuclear fuel assemblies [67][68]. A total of 14 promising detection techniques, covering passive and active measurements including both γ-ray and neutron detection, were identified within NGSI−SF. A review of these systems is given in [69]. Most of the results obtained within the NGSI−SF were based on results of simulations and only a few systems were tested under industrial conditions. In this section passive NDA systems that are routinely used or that have been tested under industrial conditions for the characterisation of spent fuel assemblies are discussed in more detail. This includes the gamma-ray spectroscopic system at Clab, the FORK detector and the Differential Die-Away Self-Interrogation (DDSI) and Passive Neutron Albedo Reactivity (PNAR) devices, which were both developed as part of the NGSI-SF.

4.1 Gamma-rays spectroscopy

Gamma-ray spectroscopy is a powerful tool to verify characteristics of spent fuel as demonstrated for spent fuel elements of research reactors [70][71][72] and assemblies of power reactors [73][74]. It is well known that independent information such as initial enrichment, burnup and cooling time can be derived by combining absolute and relative activity ratios of some key radionuclides such as ^{134}Cs, ^{137}Cs and ^{154}Eu [75][76][77][78][79]. This is due to difference in production process and half-life of these radionuclides [75][77]. Evidently, the information that can be retrieved depends on the cooling time.

Most of the gamma-ray spectroscopic systems rely on the use of High Purity Germanium (HPGe) detectors. The potential of Cadmium Zinc Telluride (CZT) semiconductor detectors operating at ambient temperature for the characterisation of spent nuclear fuel is discussed in [80]. CZT detectors also offer the possibility to perform gamma-ray spectroscopic measurements and separate the contribution from ^{134}Cs, ^{137}Cs and ^{154}Eu. Detection systems using CZT detectors to verify spent fuel assemblies in storage ponds have been developed and are used for routine safeguards inspections [81][82]. The use of scintillations detectors for gamma-ray spectroscopy has been limited by their reduced energy resolution. In recent years, the introduction of lanthanum bromide ($LaBr_3$) scintillation detectors feature higher energy resolution than traditional sodium iodide (NaI) detectors and the ability to work at high count rates. The impact of the resolution of different gamma-ray detectors is illustrated in Figure 16 that compares spectra of a ^{207}Bi source taken with a HPGe, CZT, $LaBr_3$, $CeBr_3$ and BGO detector.

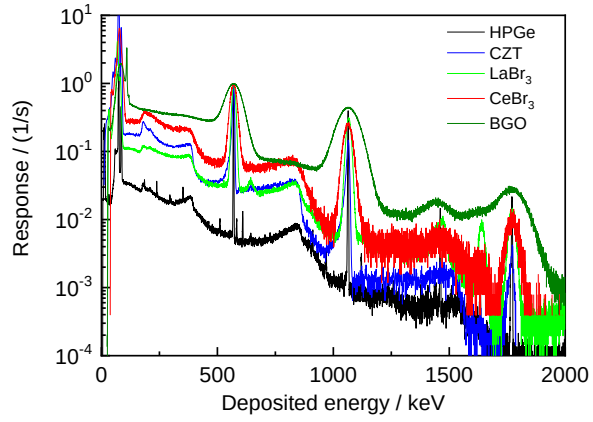

Figure 16 – Comparison of spectra obtained from measurements with different detectors (HPGe, CZT, $LaBr_3$, $CeBr_3$ and BGO) using a ^{207}Bi radionuclide source.

At Clab a gamma-ray spectroscopic scanning system using an HPGe detector is installed [79] [83]. A schematic representation of the system is shown in Figure 17 – Schematic representation of the experimental set-up for gamma-ray spectroscopic measurements at the Clab facility. Figure taken from [79]. It includes a mechanical scanning system installed in the pool that can move the assembly vertically and rotate it around its central axis. A 1.9 m thick concrete wall separates the pool from the location where the detector is placed. The detector is located at about 2.5 m from the centre of the assembly. Within the concrete wall there is an air-filled collimator with a horizontal width such that the full assembly in the horizontal plane is viewed and with a vertical width of 5 mm to arrive at an axial resolution of about 15 mm. A steel plate separates the pool and the collimator. Attenuation plates can be inserted at the end of the collimator to reduce the impact of the gamma-ray on the dead time of the detection system. Experiments are mostly carried out with one corner facing the detector as illustrated in Figure 18.

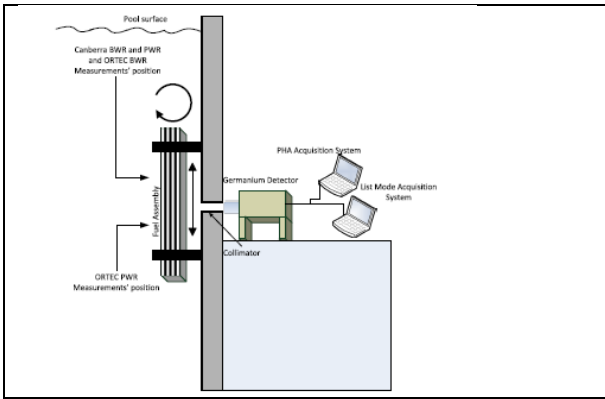

Figure 17 – Schematic representation of the experimental set-up for gamma-ray spectroscopic measurements at the Clab facility. Figure taken from [79].

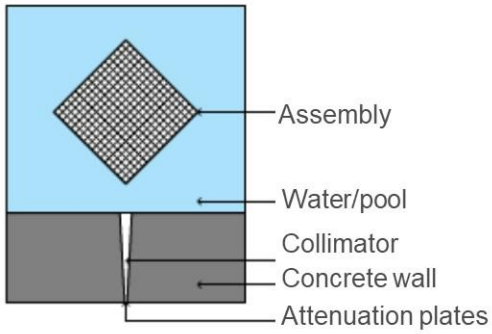

Figure 18 – Schematic representation of the measurement configuration at the gamma-spectroscopic system at Clab with the one corner of the assembly facing the opening of the collimator. Note that the dimensions are not to scale, as the collimator is longer than the side of an assembly. Figure taken from [85].

Several measurement campaigns using this system have been carried out [74][77][79][83][84]. Results obtained from part of these measurements were used by Solans et al. [85] to test an intrinsic self-calibration method to determine the relative abundances of radionuclides and to perform an uncertainty evaluation. This work was part of WP8. Such a self-calibration method, which is routinely used in nuclear safeguards to determine the isotopic composition of nuclear materials (see e.g. [86]), relies on the use of multiple full-energy peaks in the gamma-ray spectrum to account for the energy dependence of the overall detection efficiency combining the gamma-ray attenuation in the sample, solid angle and intrinsic detection efficiency. In case of spent fuel the method can be used to derive the activity ratio of ^{134}Cs and ^{154}Eu relative to the one of ^{137}Cs, as already demonstrated in [87]. Evidently, due to the relatively short half-life of ^{134}Cs and ^{154}Eu the method is not applicable for long cooling times. The results obtained by Solans et al. [85] illustrate that the activity ratios ^{134}Cs/^{137}Cs and ^{154}Eu/^{137}Cs obtained from two different measurement campaigns with different measurement conditions are in better agreement when applying a self-calibration method. In addition, it is shown that for a given assembly type and experimental configuration the variation of the energy dependence of the overall detection efficiency does not strongly vary from one assembly to another. The horizontal positioning of the assembly with respect to the opening of the collimator has a strong impact due to heterogeneous radial distributions of the radionuclides in the assembly. The impact of heterogeneous distributions is reduced by combining results of measurements with each of the four edges of the assembly facing the detector. Another systematic effect is the position of the assembly, in particular, the distance between assembly and collimator which will have an influence on the gamma-ray attenuation in the water. A change of 1 cm in distance changes the count rate with 10%. This will not affect activity ratios in case a self-calibration is applied, however, it will have an impact on the determination of the absolute activity of ^{137}Cs.

An attempt was made by Solans et al. [85] to verify the consistency of the detector response obtained from different measurement campaigns by comparing directly the net peak areas of observed full energy peaks. Such a comparison requires a detailed knowledge of the measurement conditions, in particular the attenuation plates that were used and the detector position. Unfortunately, this information was not available. Therefore, only a relative consistency verification can be done. The net peak areas of the 661 keV full energy peak derived from two different measurement campaigns were compared. The pooled standard deviation of the ratio resulting from measurements is 2.2% and 3.9% for BWR and PWR assemblies, respectively. A similar consistency check is shown in Figure 19, which plots the ratio of net peak areas for the 661 keV full energy peak derived by Solans et al. [85] and the one of Vaccaro et al. [79] as a function of burnup for a set of PWR and BWR assemblies. The net peak areas obtained in by Vaccaro et al. [79] and Solans et al. [85] result from an analysis by two different persons using results of different experiments with different attenuation plates and a different analysis codes. In addition, the data of Solans et al. [85] are derived from a spectrum that is the results of an integration over the axial length of the assembly. The integration limits correspond approximately to the boundaries of the burnup plateau. The spectra analysed by Vaccaro et al. [79] are obtained from measurements corresponding to the burnup plateau. For the PWR assemblies the ratio is rather constant and there is no obvious dependence with assembly type. The relative standard deviation of the ratio of the two data sets is 1.5 % for the PWR assemblies. For the BWR assemblies a stronger impact of the assembly type is observed, with the largest deviation for the two 8 × 8 Type 2 assemblies. For these assemblies the relative standard deviation derived from the 4 corner measurements was more than 10% for both the data of Solans et al. [85] and Vaccaro et al. [79]. This suggest strong heterogeneous irradiation conditions. Excluding the results of these two assemblies, a pooled relative standard deviation of 1.5% is obtained from the standard deviations for the 10 × 10 and 8 × 8 type of assemblies. To clarify the difference in average ratio between the 10 × 10 and 8 × 8 type of assemblies further studies are required.

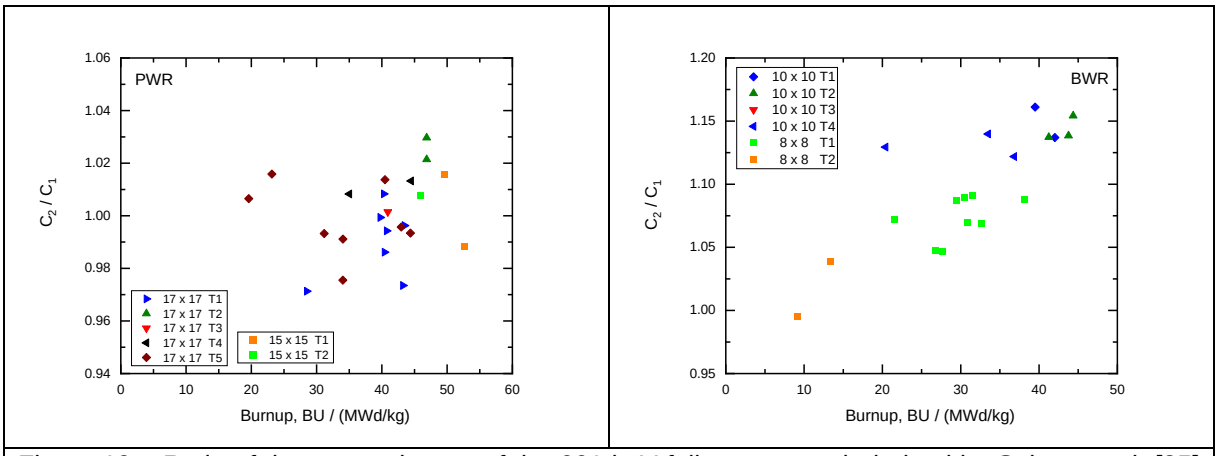

Figure 19 – Ratio of the net peak area of the 661 keV full energy peak derived by Solans et al. [85] (C2) and Vaccaro et al. [79] (C1) as a function of burnup. The net peak area is the sum of the areas from the four corner measurements. The data for different assembly types for both PWR (left) and BWR (right) assemblies are indicated with a different symbol and colour.

Bengtsson et al. [84] derived an absolute activity for ^{137}Cs present in the assembly by calibrating the gamma-ray spectroscopic detection system Clab with a reference ^{137}Cs radionuclide source and by applying a geometrical correction factor based on results of Monte Carlo simulations with Geant4. They observed a good linear relationship between the measured activity and the one calculated with the SNF depletion code. However, the average ratio of the calculated and experimental activity was 1.39 with a relative standard deviation of 3.3%. The average ratio of 1.39 is most probably due to an underestimation of the experimental activity and more studies are required to clarify this difference. Therefore, at present absolute activities can only be derived from gamma-ray spectroscopic measurements at Clab after calibrating the system with an assembly with a known ^{137}Cs inventory.

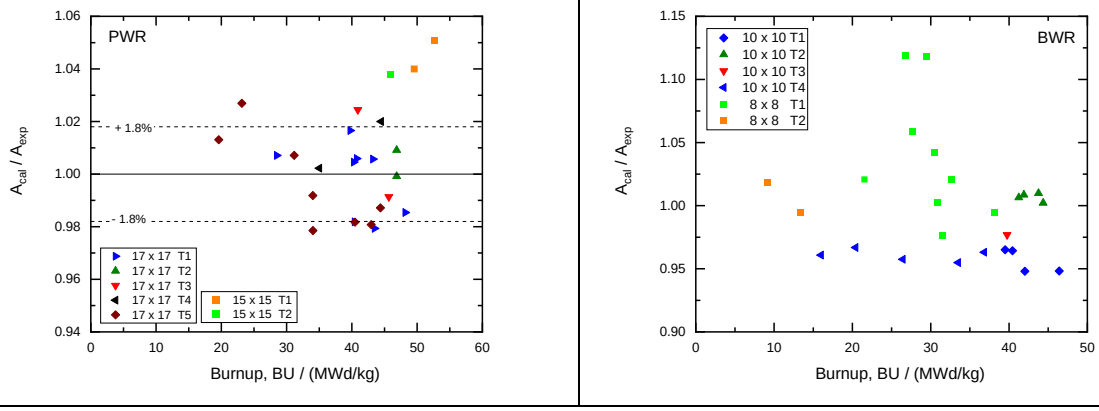

Figure 20 – Ratio of the calculated and experimental ^{137}Cs activity as a function of burnup. The calculation activity was normalised. Data for different assembly types for both PWR (left) and BWR (right) are indicated with a different symbol and colour.

A similar exercise was done within WP8 by comparing the measured full energy net peak areas for the 661 keV gamma-ray from ^{137}Cs derived by Vaccaro et al. [79] with the ^{137}Cs activity calculated with the Serpent code. That means that the experimental net peak area is compared with the activity and not with a calculated response which includes the gamma-ray transport in the assembly. The activity calculations were based on a single node 2D lattice representation and the average assembly burnup was used to normalise the calculation. The ratio of the calculated and experimental activity for the PWR and BWR assemblies is shown in Figure 20. The data are obtained after normalising the experimental data with a factor based on an average ratio for the PWR and BWR assemblies separately. There is a systematic difference between the ratio for the PWR 17 × 17 and 15 × 15 assemblies. This difference can most probably be reduced by including a gamma-ray transport calculation. The relative standard deviation for the 17 × 17 PWR assemblies is about 1.8%, which is a factor 1.8 smaller compared to the one reported by Bengtsson et al. [84]. For the BWR assemblies the ratio clearly depends on the fuel type. There is a systematic difference between the 10 × 10 Type 2 assemblies and the other 10 × 10 types. Neglecting the Type 2 data a relative standard deviation of 1.0 % is derived for the ratio of the calculated and experimental activity for the 10 × 10 BWR assemblies. As mentioned by Jansson et al. [74] there is a strong suspicion that the 10 × 10 assemblies were more evenly irradiated compared to the 8 × 8 assemblies. Therefore, the larger scattering of the 8 x 8 assemblies is most probably due strong heterogeneous irradiation conditions, which is amplified by normalising calculations with the average burnup and comparing with data taken from the burnup plateau.

The results discussed in this section demonstrate that the gamma-ray spectroscopic measurement system at Clab is a powerful NDA system to verify fuel input data. At present the ^{137}Cs activity (or inventory) can be derived with an uncertainty of 2% assemblies, provided that system is calibrated with a representative assembly. In addition, it offers the possibility to determine the ^{134}Cs/^{137}Cs and ^{154}Eu/^{137}Cs inventory ratios and the ^{137}Cs activity profile. An example of such a profile for a PWR assembly that was irradiated to a total burnup of 35 MWd/kg is shown in Figure 21. Including the information of such a profile in the burnup calculations will reduce systematic errors in the calculations due to the normalisation on an average burnup. However, further studies are strongly recommended to investigate the problem to calibrate the system starting from measurements with a radionuclide source and the differences observed for the different fuel types in particular for the BWR type of assemblies.

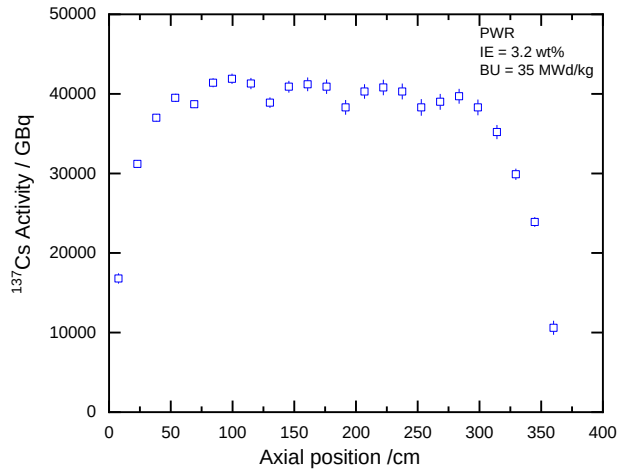

Figure 21 – The ^{137}Cs activity as a function of axial position. The activity is derived from the 661 keV full energy peak obtained from measurements with a HPGe detector. The data are from scanning measurements of a PWR fuel assembly with the system installed at the Clab facility. Data from [85].

4.2 Total neutron and gamma-ray counting by a FORK type detector

Detection of the total number of neutrons emitted by spent fuel is a common NDA method for nuclear safeguards inspection of spent fuel assemblies and to verify the burnup for nuclear criticality safety applications. It is the basis of the FORK type of detectors. The original device, designed by LANL, contains fission and ionisation chambers for total neutron counting and gamma-ray counting, respectively [87][88][89]. In variants of the original LANL design described in e.g. [90], the ionisation chambers are replaced by CZT detectors offering the possibility to perform gamma-ray spectroscopic measurements.

A FORK-type of detector was designed and constructed by SCK CEN for use at the Nuclear Power Plants (NPPs) of Tihange and Doel (in Belgium) [91]. The main objective was to assess the burnup of spent fuel assemblies upon shipments of the assemblies to the reprocessing plant of La Hague (France). This detector, shown in Figure 22, consists of two cadmium wrapped high density polyethylene arms containing each one fission chamber and one ionisation chamber to measure opposite sides of the assembly. The ionisation chambers, which are operated in current mode, measure the total gamma-ray emission by the assembly. The neutron detectors are fission chambers loaded with uranium highly enriched in ^{235}U. They are operated in pulsed mode. The cadmium around the polyethylene absorbs neutrons that are thermalised in the water such that the fission chambers are mainly sensitive to epi-thermal and fast neutrons. The whole body is placed in a stainless-steel housing and mounted on a support that is compatible with the dimensions of storage racks at the NPP of Doel. The system allows an axial scanning of the neutron emission profile by moving the assembly. An example is shown in Figure 23 [91]. This profile is obtained from an experimental campaign at the NPP of Doel of UO_2 assemblies irradiated in a PWR covering a burnup between 11 MWd/kg and 49 MWd/kg and a cooling time between 1.5 a and 10 a [91]. Such profiles can be used to verify or determine the midpoint burnup from the average assembly burnup provided by the operator.

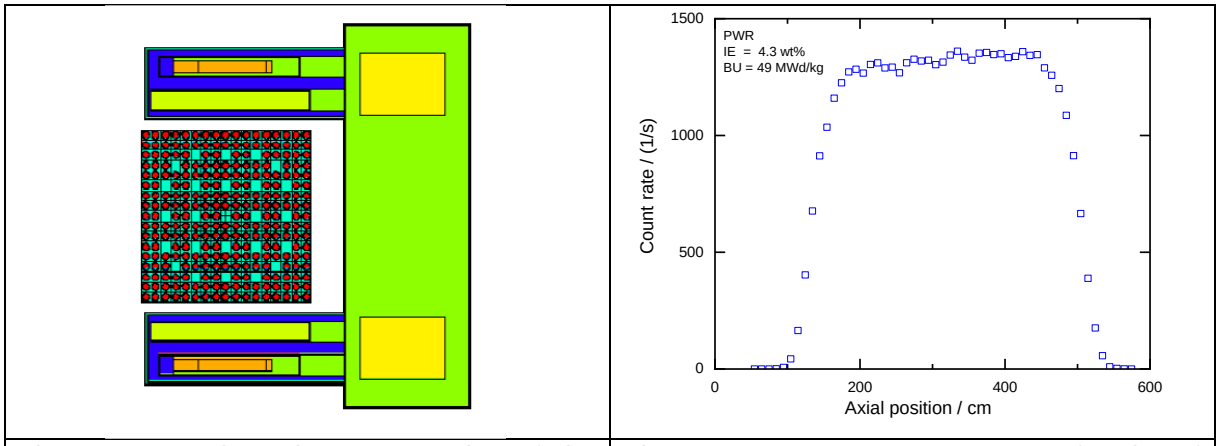

Figure 22 – Schematic representation of the FORK-type detector developed by SCK CEN for in pool spent fuel measurements at the NPPs of Tihange and Doel. Figure taken from [92].

Figure 23 – Neutron count rate as a function of axial position. The results are obtained from measurements with a FORK-type detector of an irradiated PWR assembly at the NPP of Doel. Data are taken from [91]

Calculations were carried out to verify the potential to predict the neutron response of a FORK-type detector [92]. The calculations are based on a combination of depletion calculations with the ORIGEN-ARP module of SCALE and neutron transport calculations with the MCNPX code. The experimental data were obtained from measurements at the axial midpoint of the assembly. The midpoint burnup was used to normalise the depletion calculations for the calculation of the nuclide inventory and related neutron production rate by ORIGEN-ARP. The neutron production rate was used in a neutron transport calculation with MCNPX to determine the response of the fission chambers. From these calculations, the effective neutron multiplication in the assembly was also derived. Figure 24 shows the primary total neutron production rate in the assembly as a function of the burnup obtained from the depletion calculations. The primary neutrons can be detected or they can induce a fission reaction in the assembly. This occurs primarily after thermalisation in the water of the pool. Each neutron induced fission reaction is followed by the emission of prompt fission neutrons. These neutrons can also thermalise and can be detected or continue a fission chain reaction. Hence, the total number of neutrons that are produced in the assembly is the product of the primary neutrons, mainly due to spontaneous fission, and the neutron multiplication factor. The effective neutron multiplication as a function of burnup is shown Figure 25. These data show the expected increase of primary neutron production with increasing burnup and decrease of multiplication with increasing burnup.

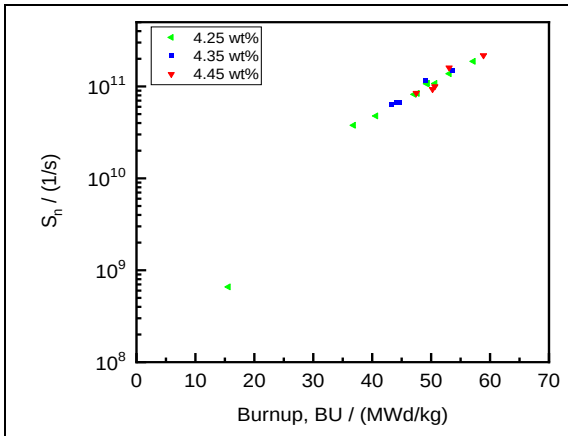

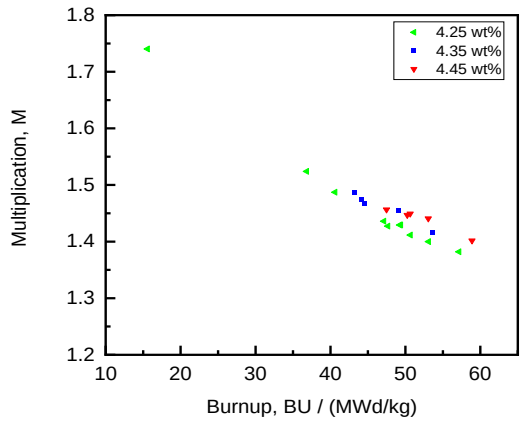

Figure 24 – Primary neutron production rate in an irradiated PWR assembly as a function of burnup. The data are representative for assemblies stored at the NPP of Doel. Data are taken from [91][92].

Figure 25 – Neutron multiplication in an irradiated PWR assembly as a function of burnup. The multiplication is for an assembly in the pool surrounded by a FORK-type detector [92].

Figure 26 shows the linear correlation between the experimental and calculated count rate. The standard deviation of the ratio of the calculated and experimental response is 3.8%. From these data one normalisation factor was derived. The data were used within WP8 to show the potential to determine the burnup from neutron measurements combined with theoretical calculations. The burnup was derived from the experimental count rate applying a linear log-log interpolation using the declared burnup as a function of the normalised theoretical response. The ratio between the experimental determined and expected burnup is shown in Figure 27. The standard deviation of this ratio is 1.25%. All data points are almost within 2%. Expanding the calculations for assemblies with different initial enrichment, burnup and cooling time it is expected that with such a procedure the burnup can be determined with an uncertainty of less than 2% for cooling times longer than 1.5 a. The proposed procedure relies on a combination of experimental data with results of calculations using one normalisation/calibration factor. This in contrast to the conventional procedure which relies only the experimental data and uses a power function to link the burnup to the neutron count rate. Since the parameters of the power function depend on the burnup, as shown in Figure 28, more calibration parameters (reference assemblies) are required.

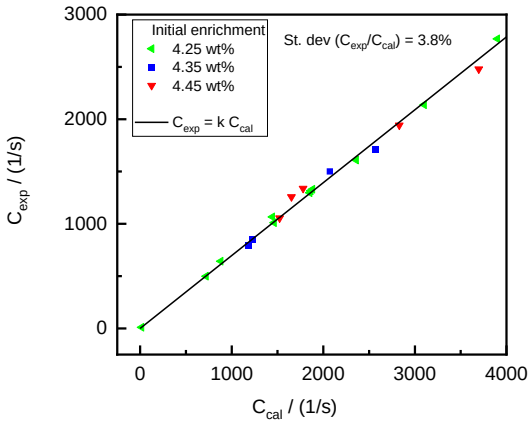

Figure 26 – Experimental count rate (C_{exp}) as a function of the calculated count rate (C_{cal}) for measurements with a FORK-type detector of PWR assemblies at the NPP of Doel. Data are taken from [91][92].

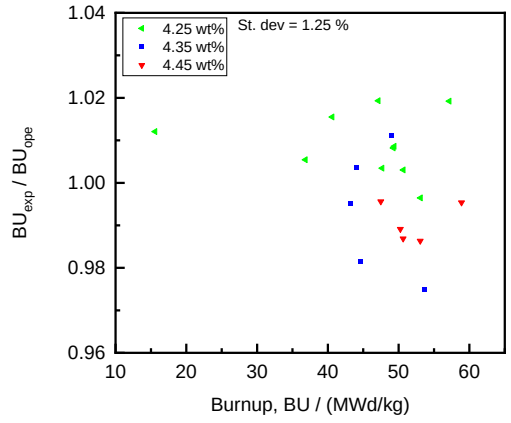

Figure 27 – Burnup of PWR assemblies derived from neutron measurements (BU_{exp}) with a FORK-type detector divided by the expected burnup (BU_{ope}). The data used to derive the experimental burnup were taken from [91][92].

Unfortunately, during the measurement campaign at the NPP of Doel the ionisation chamber of FORK detector was not functioning properly. To demonstrate the complementarity of results derived from the neutron and gamma-ray detector theoretical calculations were performed. For these calculations the spent fuel library of [93] was used. Part of the results are shown in Figure 29. For a given cooling time the response of the neutron detector is plotted as a function of the response of the gamma-ray detector. The data show that a difference in cooling time can be identified based a combination of the neutron and gamma-ray response. Therefore, the combined use of neutron and gamma-ray detection to verify assemblies prior to loading in a cask or canister can be recommended. Given that no real efforts have been made to improve both the performance of FORK-type detectors and the performance of codes to calculate the neutron emission rate of spent fuel assemblies and the neutron and gamma-ray response of such a detection system, there is even place for improvement.

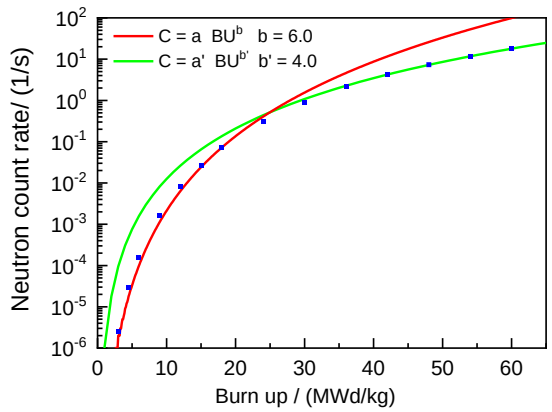

Figure 28 – Expected count rate in a FORK-type detector for measurements with irradiated PWR assemblies. The data are from simulations [14].

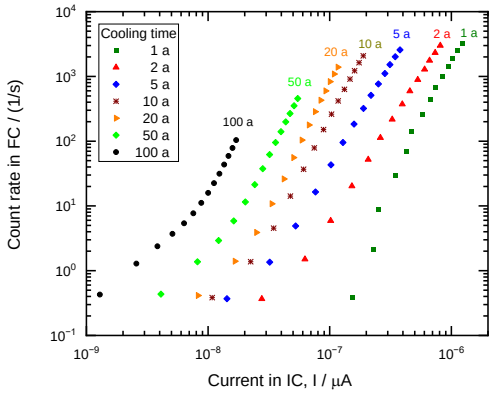

Figure 29 – Neutron count rate as a function the current in the ionisation chamber for irradiated spent fuel assemblies with an initial enrichment of and burnup between and MWd/kg. The data are from theoretical calculations using the spent fuel library of [93].

4.3 DDSI and PNAR

The DDSI and PNAR concepts were both developed at the Los Alamos Laboratory (LANL, USA) as part of the NGSI-SF with the objective to derive characteristics of a spent fuel assembly that are complementary to the total neutron emission rate, ideally an observable that is sensitive to the amount of fissile material present in the sample.

DDSI

The DDSI concept is inspired by the Differential-Die Away (DDA) [94][95] technique which is an active NDA system based on correlated neutron detection using a pulsed external neutron source. The DDSI technique is a passive NDA technique that uses the neutrons spontaneously emitted by the assembly as an internal interrogating neutron source [96]. The main idea is to provide an experimental observable that is sensitive to the neutron multiplication factor M, which can be considered as a measure of the total amount of fissile material in the fuel.

The DDSI instrument that was developed by LANL and used at Clab [97] is schematically represented in Figure 30. Neutrons emitted by the assembly are detected by an array of ^{3}He proportional counters surrounding the assembly and the time correlation technique is applied to construct a Rossi-alpha distribution. The detection system consists of four rectangular modules. Each module is made of a block of high-density polyethylene with cylindrical slots hosting 14 ^{3}He proportional counters. An additional slot can be used for an additional detector, e.g. an ionisation chamber for total gamma-ray counting. The block of polyethylene is surrounded by a cadmium sleeve to absorb neutrons that are thermalised in the water. This will reduce the die-away time of the detected neutrons. A lead shield is placed between the detector block and the assembly to reduce the gamma-ray background in the detectors. The signals of each detector are registered in list mode and the list mode data are used to obtain the Rossi-alpha distribution together with the total number of detected neutrons. The Rossi-alpha distribution is constructed by registering in coincidence the number of detected events in time windows that are opened by each detected event. An example of such a Rossi-alpha distribution is shown in Figure 31.

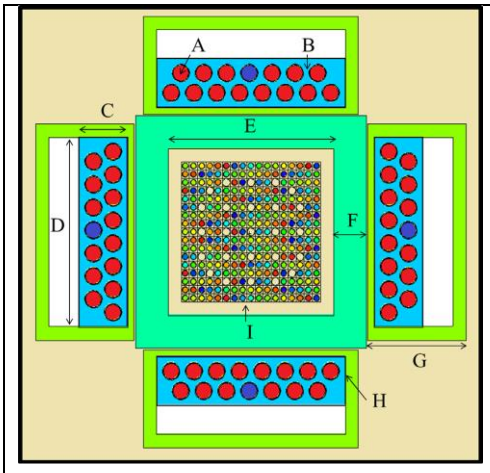

A	^{3}He detector
B	Detector pitch
C	Polyethylene
D	Polyethylene
E	Lead
F	Lead
G	Steel
H	Cd-liner surrounding polyethylene
I	Fuel assembly

Figure 30 – Schematic representation of the DDSI instrument used for measurements at the Clab facility. The figure is taken from Kaplan et al. [97].

In the procedure applied by LANL one decay constant is derived by parameterising the Rossi-alpha distribution with a single-exponential distribution in one time window in the early time domain:

$$R_{\alpha}(t) = a_e\, e^{-\frac{t}{\tau_e}}, \quad (14),$$

Such a parameterisation is shown in Figure 31. The distribution in Figure 31 is obtained from simulations described in [99]. The resulting die-away time (τ_e) can be related to the neutron multiplication in the assembly as demonstrated by Trahan et al. [98] using experimental data resulting from experiments performed at Clab.

The potential to derive additional information from a DDSI measurement by parameterising the Rossi-alpha distribution using a sum of two exponential distributions was investigated within WP8 by Solans et al. [99]. The results of this study are based on data produced by simulations combining depletion calculations using Serpent with neutron transport calculations using MCNP6. The DDSI response was calculated for a set of 17 × 17 irradiated PWR assemblies with identical rods covering an initial enrichment from 1.5 wt% to 6 wt%, a burnup from 5 MWd/kg to 70 MWd/kg and a cooling time from 2.5 a to 55 a [99]. Results are summarised in Figure 31, Figure 32 and Figure 33. The data in Figure 31 illustrate that the Rossi-alpha distribution can be described by a sum of two exponentials:

$$R_{\alpha}(t) = a_f\, e^{-\frac{t}{\tau_f}} + a_s\, e^{-\frac{t}{\tau_s}}, \quad (15),$$

consisting of a component with a fast (τ_f) and slow (τ_e) die-away time constant.

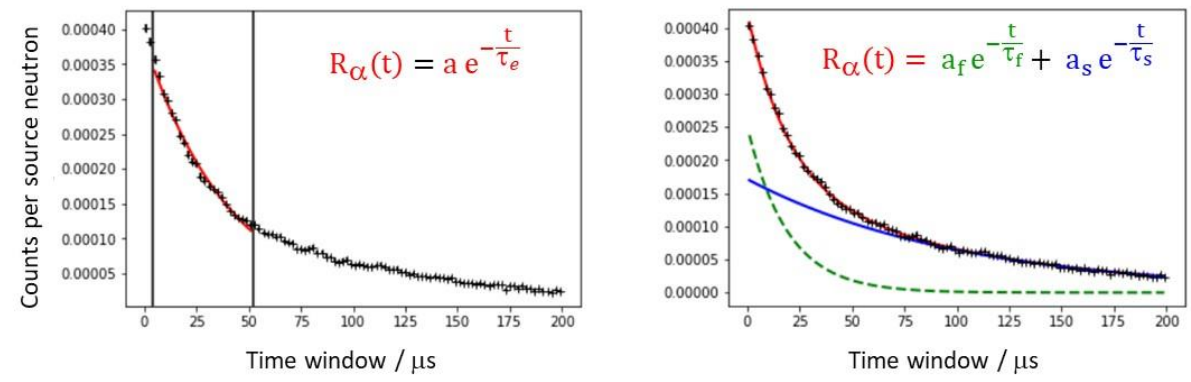

Figure 31 – Rossi-alpha distribution parameterised with a single (left) and double (right) exponential distribution. The Rossi-alpha distribution is derived from simulations for a UO_2 PWR assembly with an initial enrichment of 1.5 wt% and irradiated to a burnup of 10 MWd/kg. The cooling time is 50 a.

A comparison of the results in Figure 32 and Figure 33 reveals the advantage of a parameterisation using two exponentials. Figure 32 shows the information that is derived from a fit with a single exponential. The total count rate is plotted as a function of the early die away time (τ_e). Differences in burnup (left) and initial enrichment (right) is made through a colour scheme. The result in Figure 32 show that it is not obvious to derive complementary characteristics of the spent fuel assembly due to the strong correlation between the total count rate and the early die-away time constant. The added value of a parameterisation with two exponentials is illustrated in Figure 33 by plotting the slow time constant (τ_s) as function of fast time constant (τ_f), again using a colour scheme to indicate differences in burnup and initial enrichment. Figure 33 demonstrates that the two die-away time constants provide independent information and together with the total neutron count rate they are sensitive to different characteristics of the irradiated fuel.

A parameterisation in terms of two exponential distribution was applied to fit the Rossi-alpha distribution obtained from the measurements with a DDSI prototype instrument at Clab. Results of these measurements were reported in [98]. Unfortunately, no obvious correlation was found between the decay constants derived from the simulated and experimental distributions [99]. Hence, at present it is hard to demonstrate the added value of the DDSI concept based on the available experimental data.

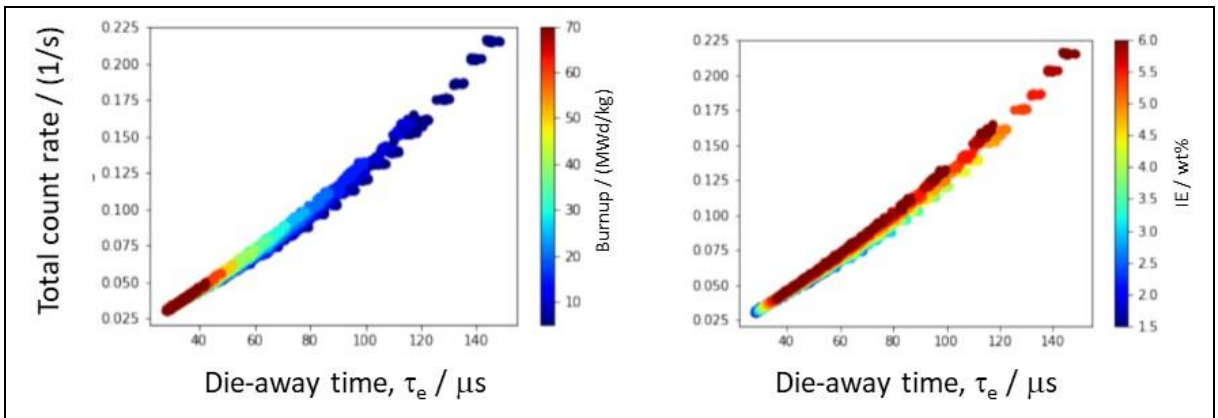

Figure 32 – Total count rate as a function of the time constant τ_e. Differences in burnup (left) and initial enrichment (right) is made through a colour scheme. Figure taken from [99].

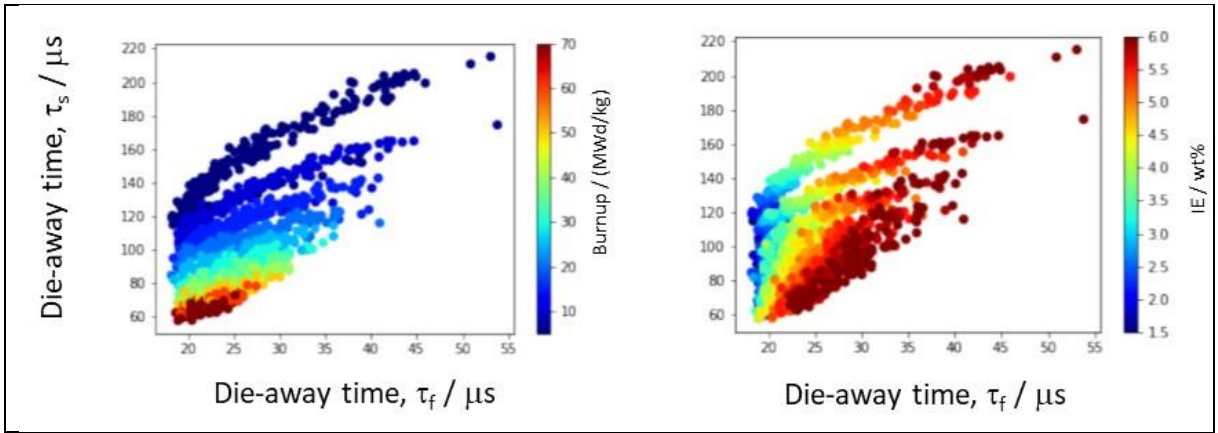

Figure 33 – Time constant τ_s as a function of the time constant τ_f. Differences in burnup (left) and initial enrichment (right) is made through a colour scheme. Figure taken from [99].

PNAR

Applying the PNAR concept, which was first proposed in [100], neutrons emitted by a spent fuel assembly are measured in two configurations, which are referred to as a high and a low multiplication configuration. The high configuration is similar to a conventional measurement with a FORK detector. However, in a PNAR device multiplication of primary neutrons by neutron induced fission in the assembly is enhanced by placing polyethylene between the assembly and detector bench. In the second configuration, neutron multiplication is suppressed by placing a cadmium sheet between the assembly and the detection system. The ratio of the count rates obtained with the two configurations is used as an additional observable to the total detected neutron count rate. This ratio, also referred to as the PNAR-ratio, is used to estimate the amount of fissile material present in the assembly [101].

A first prototype was built and tested on MOX fuel assemblies irradiated in the Fugen reactor in Japan [102][103]. The results of these field tests showed a promising correlation between the amount of fissile material present in the fuel and the PNAR-ratio. However, measurement times of a few hours per assembly were needed [102][103].

More recently, a PNAR device was constructed and it was tested in Finland using BWR fuel irradiated in the NPP of Olkiluoto [104][105]. This device will be part of an integrated NDA system to verify spent fuel assemblies in Finland prior to disposal [105]. It consists of four rectangular detection modules made of polyethylene. Each module contains an ionisation chamber filled with xenon and one ^{3}He proportional counter. Each polyethylene module is covered by cadmium and a lead shield is used to attenuate the gamma-radiation emitted by the assembly. To alternate between the low and high multiplication configuration a movable Cd liner is placed between the fuel guide channel and the central opening of the PNAR device. The results of the test measurements in Finland show that the PNAR-ratio can be used to distinguish between a fully irradiated assembly and an assembly not containing any fissile material [105]. However, the results do not provide evidence that the PNAR-ratio can be considered as a complementary observable to estimate a quantitative characteristic of the spent fuel in addition to the total neutron emission rate.

5. Summary and conclusions

Principles of NDA methods to characterise spent nuclear fuel were discussed. A distinction was made between methods to produce accurate data for code validation and methods to determine characteristics of spent fuel assemblies under industrial operation. The latter are used to verify fuel related input data that are needed as input for depletion calculations. The main signatures that can be used for NDA of spent nuclear fuel, i.e. decay heat and neutron and gamma-ray emission characteristics, were discussed. The key radionuclides producing these signatures were identified and recommended decay data, required to calculate the signatures, were specified. In the overview of NDA methods and devices progress or improvements made as part of WP8 of EURAD were emphasised.

Within WP8 two activities concentrated on the production of accurate experimental data for code validation. An absolute NDA method to determine the production rate of spontaneous fission neutrons by spent fuel was developed. The method was demonstrated by measurements of a spent fuel segment at the LHMA facility of SCK CEN. The results provide high quality data to test the performance of depletion codes to predict the neutron output or ^{244}Cm inventory. The second contribution was the study of the calorimeter at Clab. This instrument determines the decay power of spent fuel assemblies. Results of these measurements are extensively used for code validation. As part of WP8 the analysis procedures were improved. The procedures include a quality control of the data. The procedures were applied to re-analyse data previously used in a blind test exercise. It was shown that the experimental decay derived with the procedure that was used for that exercise suffers from a systematic error. The new procedure was applied to derive the decay power of a set of PWR and BWR assemblies that are part of the SKB-50 campaign. Results obtained using the procedures defined within WP8 are fully consistent with results that were independently derived as part of an EPRI project. The present procedures reduce the uncertainty of the decay heat measurements by a factor 2 to less than 2%.

The performance of the gamma-ray spectroscopic system at Clab was verified using data from experimental campaigns that were carried out in the past. It was demonstrated that with this system characteristics of spent fuel assemblies such as the ^{137}Cs activity and activity ratios for ^{134}Cs/^{137}Cs and ^{154}Eu/^{137}Cs together with their axial profiles can be determined. In case the system is calibrated with a representative assembly, the ^{137}Cs activity can be derived with an uncertainty of about 2%. The axial activity profile of ^{137}Cs is a valuable input for any depletion calculation to verify assumption made about the fuel burnup. However, the performance of the system can be improved by a gamma-ray transport calculation to better understand the difference in response for different fuel types and to allow for an absolute determination of the ^{137}Cs activity.

Literature data resulting from measurements of PWR assemblies at the NPP of Doel were used to study the potential of neutron detection for the characterisation of fuel assemblies using a FORK-type detection system. The study revealed that the neutron response of such a detector can be calculated combining depletion calculations to predict the primary neutron production in the fuel with a neutron transport calculation to account for the neutron multiplication in the fuel and the detection probability in the fission chambers. It was demonstrated that by combining experimental data with theoretical calculated detector responses the average burnup of an assembly can be determined with an uncertainty of about 2%. The main constraint is the calibration of the detection system with at least one reference assembly.

The performance of two other passive neutron-based NDA systems, i.e. PNAR and DDSI, was investigated. Compared to the conventional FORK-type detection system the PNAR concept provides in addition to the total neutron and gamma-ray response the so-called PNAR-ratio. This PNAR-ratio can be used to distinguish between a fully irradiated assembly and an assembly not containing any fissile material. At present, no real complementary observable can be derived to obtain a quantitative characteristic, in addition to the neutron count rate. A study of the DDSI concept based on simulated data suggests that the analysis procedure that is currently applied can be improved so that from measurements with such a device, more information about the spent fuel characteristics can be

retrieved. Unfortunately, the quality of the experimental data taken at the Clab facility with a prototype device is not good enough to confirm these findings.

References

[1] Marcus Seidl, Peter Schillebeeckx and Dimitri Rochman, “On the potential to increase the accuracy of source term calculations for spent nuclear fuel”, Frontiers in Energy Research

[2] A. Stankovskiy and G. Van den Eynde, Advanced Method for Calculations of Core Burn-Up, Activation of Structural Materials, and Spallation Products Accumulation in Accelerator-Driven Systems, Science and Technology of Nuclear Installations, 2012 (2012) 545103 https://doi.org/10.1155/2012/545103

[3] Brandon P. Haugh and Rodolfo M. Ferrer, “CASMO5 PWR Methods and Validation Report”, Studsvik, SSP-14-P01/012-R, Rev.1, 2015

[4] H. Joshua and R. Joel, “Validation of CASMO5 spent fuel isotopics with decay and fission yield uncertainties”, Proceedings of the International Conference on Physics of Reactors (PHYSOR 2014), September 28 – October 3, 2014, The Westin Miyako, Kyoto, Japan.

[5] A. Tsilanizara, C. M. Diop, B. Nimal, M. Detoc, L. Lunéville, M. Chiron, T. D Huynh, I. Brésard, M. Eid, J. C. Klein, B. Roque, P. Marimbeau, C. Garzenne, J. M. Parize & C. Vergne, “DARWIN: An Evolution Code System for a Large Range of Applications”, Journal of Nuclear Science and Technology, 37 (supplement 1) (2000) 845-849, DOI: 10.1080/00223131.2000.10875009

[6] F. Álvarez-Velarde, E.M. González-Romero, I.M. Rodríguez, ”Validation of the burn-up code EVOLCODE 2.0 with PWR experimental data and with a Sensitivity/Uncertainty analysis”, Annals of Nuclear Energy, 73 (2014) 175–188

[7] J. Leppänen, M. Pusa, T. Viitanen, V. Valtavirta, T. Kaltiaisenaho, “The Serpent Monte Carlo code: Status, development and applications in 2013”, Annals of Nuclear Energy 82 (2015) 142-150

[8] Riku Tuominen, Ville Valtavirta, Jaakko Leppänen, “New energy deposition treatment in the Serpent 2 Monte Carlo transport code”, Annals of Nuclear Energy 129 (2019) 224 – 232

[9] Teodosi Simeonov and Charles Wemple, “Advances in Studsvik’s system for spent fuel analyses”, EPJ Web of Conferences 247 (2021) 02021

[10] B.T. Rearden and M.A. Jessee, “SCALE Code System Version 6.2.2”, Report ORNL/TM-2005/39, Oak Ridge National Laboratory, February 2017 https://info.ornl.gov/sites/publications/Files/Pub72982.pdf

[11] H. Ferroukhi, K. Hofer, J-M. Hollard, A. Vasiliev and M.A. Zimmerman, “Core Modelling and Analysis of the Swiss Nuclear Power Plants for Qualified R&D Applications”, in Proc. Int. Conf. on the Physics of Reactors, PHYSOR’08, Interlaken, Switzerland

[12] O. Leray, H. Ferroukhi, M. Hursin, A. Vasiliev, D. Rochman, “Methodology for core analyses with nuclear data uncertainty quantification and application to Swiss PWR operated cycles”, Annals of Nuclear Energy 110 (2017) 547 - 559

[13] JCGM/WG 1, Evaluation of measurement data - Guide to the Expression of Uncertainty in Measurements, JCGM 100:2008, September 2008. https://www.bipm.org/en/committees/jc/jcgm/publications

[14] G. Žerovnik, P. Schillebeeckx, K. Govers, A. Borella, D. Ćalić, L. Fiorito, B. Kos, A. Stankovskiy, G. Van den Eynde and M. Verwerft, "Observables of interest for the characterisation of Spent Nuclear Fuel", JRC Technical Reports, EUR 29301 EN, 2018

[15] Decay Data Evaluation Project, http://www.nucleide.org/DDEP_WG/DDEPdata.htm

[16] P. Santi and M. Miller, “Reevalaution of prompt neutron emission multiplicity distributions for spontaneous fission”, Nuclear Science and Engineering 160 (2008) 190 – 199

[17] W.B. Wilson, R.T. Perry, E.F. Shores, W.S. Charlton, T.A. Parish, G.P. Estes, T.H. Brown, E.D. Arthur, M. Bozoian, T.R. England, D.G. Madland and J.E. Stewart, “SOURCES 4C: A code for calculating (alpha,n), spontaneous fission and delayed neutron sources and spectra”, LANL Report, LA-UR-02-1839, April 2002

[18] W.B. Wilson, R.T. Perry, W.S. Charlton and T.A. Parish, “Sources: A code for calculating (alpha,n), spontaneous fission, and delayed neutron sources and spectra”, Progress in Nuclear Energy 51 (2009) 608 – 613

[19] G.S. Boykov, B.G. Gerasimenko, V.D. Dmitriev, L.V. Drapchinsky, O.I. Kostochkin, K.A. Petrzhak, B.M. Shiryaev and V.A. Trenkin, “Precision prompt neutron spectrum measurements of minor actinides for transmutation problem”, Proceedings International Conference on Nuclear Data for Science and Technology, Trieste, Italy, 1997, Vol. 2, pp. 1310, 1997

[20] P.M. Rinard, G.E. Bosler and J.R. Phillips, “Calculated Neutron-Source Spectra from Selected Irradiated PWR Fuel Assemblies”, LANL Report, LA-9125-MS, December 1981

[21] B.L. Broadhead, M. D. DeHart, J.C. Ryman, J.S. Tang, C.V. Parks, Investigation of Nuclide Importance to Functional Requirements Related to Transport and Long-Term Storage of LWR Spent Fuel, Report ORNL/TM-12742, Oak Ridge National Laboratory, June 1995

[22] I.C. Gauld and J.C. Ryman, Nuclide Importance to Criticality Safety, Decay Heating, and Source Terms Related to Transport and Interim Storage of High-Burnup LWR Fuel, Report NUREG/CR-6700 (ORNL/TM-2000/284), U.S. Nuclear Regulatory Commission, Oak Ridge National Laboratory, January 2001

[23] OECD NEA, Evaluation Guide for the Evaluated Spent Nuclear Fuel Assay Database (SFCOMPO), Nuclear Science, NEA/NSC/R(2015)8, February 2016

[24] F. Michel-Sendis, I. Gauld, J.S. Martinez, C. Alejano, M. Bossant, D. Boulanger, O. Cabellos, V. Chrapciak, J. Conde, I. Fast, M. Gren, K. Govers, M. Gysemans, V. Hannstein, F. Havlu, M. Hennebachj, G. Hordosy, G. Ilas, R. Kilger, R. Mills, D. Mountford, P. Ortego, G. Radulescu, M. Rahimi, A. Ranta-Aho, K. Rantamäki, B. Ruprecht, N. Soppera, M. Stuke, K. Suyama, S. Tittelbach, C. Tore, S. Van Winckel, A. Vasiliev, T. Watanabe, Toru Yamamoto, Toshihisa Yamamoto, SFCOMPO-2.0: An OECD NEA database of spent nuclear fuel isotopic assays, reactor design specifications, and operating data, Annals of Nuclear Energy 110 (2017) 779 – 788

[25] I. Matsson and B. Grapengiesser, “Developments in Gamma Scanning of Irradiated Nuclear Fuel”, Applied Radiation Isotopes, 48 (1997) 1289 - 1298

[26] Stefaan Van Winckel, Rafael Alvarez-Sarandes, Daniel Serrano Purroy and Laura Aldave de las Heras, “Assay data of spent nuclear fuel: the lab-work behind the numbers”, Frontiers in Energy Research 11 (2023) 1168460

[27] J. Eysermans, M. Verwerft, K. Govers, R. Ichou, G. Ilas, U. Meryturek, N. Messaoudi, P. Romojaro and N. Slosse, “REGAL International Program, Analysis of experimental data for depletion code validation”, Annals of Nuclear Energy 172 (2022) 109057

[28] J. Eysermans and M. Verwerft, “Databook of flat burnup samples from rod D05 extracted from fuel assembly FT1X57, Tihange 1 NPP”, Report R-8189 (rev.1), SCK CEN November, 2022

[29] K. Lemmens, E. González-Robles, B. Kienzler, E. Curti, D. Serrano-Purroy, R. Sureda, A. Martínez-Torrents, O. Roth, E. Slonszki, T. Mennecart, I. Günther-Leopold, Z. Hózer, “Instant release of fission products in leaching experiments with high burn-up nuclear fuels in the framework of the Euratom project FIRST- Nuclides”, J. Nucl. Mater. 484 (2017) 307-323.

[30] T. Mennecart, L. Iglesias, M. Herm, T. König, G. Leinders, C. Cachoir, K. Lemmens, M. Verwerft, V. Metz, E. González-Robles, K. Meert, T. Vandoonre, R. Gaggiano, , “Effect of hydrogen gas

and leaching solution on the fast release of fission products from two PWR fuels", Journal of Nuclear Materials, 588 (2024) 154811

[31] M. Verwerft, B. Vos, S. Van den Berghe, K. Govers, "First Nuclides Post-Irradiation Examination report Rod D05 - OM1", SCK•CEN, Mol, report R-5579 (2014)

[32] P. Schillebeeckx, M. Verwerft, G. Žerovnik, Y. Parthoens, B. Pedersen, G. Alaerts, G. Cools, K. Govers, J. Paepen, G. Varasano and R. Wynants, "A non-destructive method to determine the neutron production rate of a sample of spent nuclear fuel under standard controlled area conditions", JRC Technical Report EUR 30379 EN, European Atomic Energy Community, Luxembourg, 2020, ISBN 978-92-76-22349-8 (where available), doi:10.2760/6148853, JRC121586

[33] P. Schillebeeckx, M. Verwerft, P. Romojaro, G. Žerovnik, N. Messaoudi, G. Alaerts, L. Fiorito, K. Govers, J. Paepen, Y. Parthoens, B. Pedersen, A. Stankovskiy, G. Van den Eynde and R. Wynants, "An absolute measurement of the neutron production rate of a spent nuclear fuel sample used for depletion code validation", Frontiers in Energy Research 11 (2023) 1162367

[34] Ana Muñoz (ENRESA/EUNSA), "Specification of measured isotopic concentrations of BWR Spent Fuel", 19 June 2020, Enresa_INF-TD-10032.pdf, Dissemination level: Subtask 2.1 modelling participants

[35] Dimitri Rochman, Alexander Vasiliev , Hakim Ferroukhi, Ana Muñoz , Miriam Vazquez Antolin , Marta Berrios Torres, Carlos Casado Sanchez, Teodosi Simeonov, and Ahmed Shama "Analysis of ENRESA BWR samples: nuclide inventory and decay heat", EPJ Nuclear Science Technology 8 (2022) 9

[36] H. Menlove, "Description and Operation Manual for the Active Well Coincidence Counter", Report LA-7823-M, Los Alamos National Laboratory, May 1979W.

[37] J. E. Swansen, "Deadtime reduction in thermal neutron coincidence counter", Nuclear Instruments and Methods in Physics Research B 9 (1985) 80 – 88

[38] James E. Swansen, Paul R. Collinsworth and Merlyn S. Krick, "Shift-Register coincidence electronics system for thermal neutron counters", Nuclear Instruments and Methods 176 (1980) 555 – 565

[39] M.S. Krick and J.E. Swansen, "Neutron multiplicity and multiplication measurements", Nuclear Instruments and Methods in Physics Research 219 (1984) 384– 393

[40] Hage and D.M. Cifarelli, "On the factorial moments of the neutron multiplicity distribution of the fission cascades", Nuclear Instruments and Methods in Physics Research A236 (1985) 165 – 177

[41] X-5 Monte Carlo Team, MCNP—A General N-Particle Transport Code, Version 5. Volume I: Overview and Theory, LA-UR-03-1987, Los Alamos National Laboratory, 2005

[42] H.J. Kim, W.I. Ko, S.Y. Lee & H.D. Kim, "The Effect of the Neutron Multiplication Factor on a Nuclear Material Measurement in Dry-Processed Spent Fuel Material", Journal of Nuclear Science and Technology, 41 (Supplement 4) (2004) 384 – 387

[43] H. Ramthum and K. Debertin, "Burn-up determination of irradiated fuels by means of their heat output", Atomkernenergie 19 (1972) 17 – 22

[44] Shigetaka Maeda, Takashi Sekine, Takafumi Aoyama, "Measurement and analysis of decay heat of fast reactor spent MOX fuel", Annals of Nuclear Energy 31 (2004) 1119 – 1133

[45] J.C. Jaboulay and S. Bourganel, "Analysis of MERCI Decay Heat Measurement for PWR UO_2 Fuel Rod", Nuclear Technology 177 (2012) 73 - 82

[46] SKB, “Measurements of Decay Heat in Spent Nuclear Fuel at the Swedish Interim Storage Facility, Clab", SKB report R-05-62, December 2006 https://www.skb.se/publikation/1472024/R-05-62.pdf

[47] B.D. Murphy and I.C. Gauld, “Spent Fuel Decay Heat Measurements Performed at the Swedish Central Interim Storage Facility”, NUREG/CR-6971, ORNL/TM-2008/016, February 2010

[48] M.A. McKinnon, J.W. Doman, C.M. Heeb and J.M. Creer, “MONTICELLO BWR spent fuel assembly decay heat predictions and measurements”, PNL – 5799, UC – 85, June 1986

[49] I.C. Gauld, G. I q, B.D. Murphy, and C.F. Weber, “Validation of SCALE5 Decay Heat Predictions for LWR Spent Nuclear Fue”l, NUREG/CR-6972, ORNL/TM-2008/015, February 2010

[50] L. San-Felice, R. Eschbach and P. Bourdot, “Experimental validation of the DARWIN2.3 package for fuel cycle applications”, Nuclear Technology 184 (2013) 217 - 232

[51] Toru Yamamoto and Daiki Iwahashi, “Validation of decay heat calculation results of ORIGEN2.2 and CASMO5 for light water reactor fuel”, Journal of Nuclear Science and Technology, 53 (2016) 2108 - 2118

[52] Wim Haeck and Raphaëlle Ichou, “Experimental validation of depletion calculations with VESTA 2.1.5 using JEFF-3.2”, EPJ Web of Conferences 146 (2017) 06012

[53] Damien Gérard, “Validation expérimentale due code ALEPH2 d’évolution du combustible pour le calcul de chaleur résiduelle”, MSc Thesis, Université catholique de Louvain, Ėcole polytechnique de Louvain, 2018.

[54] Bamidele Ebiwonjumi, Sooyoung Choi, Matthieu Lemaire, Deokjung Lee, Ho Cheol Shin, Hwan Soo Lee, “Verification and validation of radiation source terms capabilities”, Annals of Nuclear Energy 124 (2019) 80 – 87

[55] Germina Ilas and Joseph R. Burns, “SCALE 6.2.4 Validation for Light Water Reactor Decay Heat Analysis”, Nuclear Technology 208 (2022) 403 – 413

[56] Ahmed Shama, Dimitri Rochman, Stefano Caruso, Andreas Pautz, “Validation of spent nuclear fuel decay heat calculations using Polaris, ORIGEN and CASMO5”, Annals of Nuclear Energy 165 (2022) 108758

[57] D. Rochman, J. Taforeau, T. Simeonov, A. Shama, “Comparison of calculated and measured spent nuclear fuel decay heat with CASMO5, *SNF* and standard methods”, Nuclear Engineering and Design, 410 (2023) 112392

[58] Peter Jansson, Martin Bengtsson , Ulrika Böckström, Francisco Álvarez-Velarde, Dušan Čalič, Stefano Caruso, Ron Dagan, Luca Fiorito, Lydie Giot, Kevin Govers, Augusto Hernandez Solis, Volker Hannstein, Germina Ilas, Marjan Kromar, Jaakko Leppänen, Marita Mosconi, Pedro Ortego, Rita Plukienė, Arturas Plukis, Anssu Ranta-Aho, Dimitri Rochman, Linus Ros, Shunsuke Sato, Peter Schillebeeckx, Ahmed Shama, Teodosi Simeonov, Alexey Stankovskiy, Holly Trellue, Stefano Vaccaro, Vanessa Vallet, Marc Verwerft, Gašper Žerovnik and Anders Sjöland, “Blind Benchmark Exercise for Spent Nuclear Fuel Decay Heat”, Nuclear Science and Engineering 196 (2022) 1125-1145

[59] I.T. Myers, “Improved Method of Gamma-Ray Calorimetry”, The Review of Scientific Instruments, 29 (1958) 758 – 761

[60] S.R. Gunn, “Radiometric calorimetry: a review”, Nuclear Instruments and Methods 29 (1964) 1 – 24

[61] S.T. Hue, T.W. Crane, W.L. Talbert, J. C. Lee, “Nondestructive assay methods for irradiated nuclear fuels”, Report LA – 6923, January 1978

[62] M. Tarvainen, F. Lévay, T.E. Valentine, M. Abhold, B. Moran, “NDA techniques for spent fuel verification and radiation monitoring”, STUK-YTO-TR 133, August 1997

[63] IAEA, “Safeguards Techniques and Equipment: 2011 Edition”, International Nuclear Verification Series No. 1 (Rev. 2), ISBN 978-92-0-118910-3 (2011)

[64] A. Lebrun, S. Jung, S. Zykov, A. Berlizov, “Status of NDA techniques in use for IAEA verification of light water reactor spent fuel”, in: Proceedings of the 54th Annual Meeting of the Institute of Nuclear Materials Management, INMM 2013, Atlanta, Georgia, July 2013.

[65] B.B. Bevard, J.C. Wagner, C.V. Parks, M. Aissa, ”Review of information for spent nuclear fuel burnup confirmation”, Report NUREG/CR-6998, December 2009

[66] A. Lebrun and G. Bignan, “Nondestructive Assay of Nuclear Low-Enriched Uranium Spent Fuels for Burnup Credit Application”, Nuclear Technology 13 (2001) 216–229

[67] S.J. Tobin, “Determination of plutonium content in spent fuel with non-destructive assay”, Presented at the 50th INMM Annual Meeting, Tucson, AZ, 11 – 17 July 2009, Report LA-UR- 09-03748 (2009).

[68] S.J. Tobin, H.O. Menlove, M.T. Swinhoe, M.A. Schear, “Next Generation Safeguards Initiative research to determine the Pu mass in spent fuel assemblies: purpose, approach, constraints, implementation and calibration”, Nuclear Instruments and Methods in Physics Research A 652 (2011) 73–75.

[69] A.M. Bolind, M. Seya, “The State of the Art of Nondestructive Assay of Spent Nuclear Fuel Assemblies – A Critical Review of the Spent Fuel NDA Project of the U.S. Department of Energy's Next Generation Safeguards Initiative”, JAEA-Review-2015-027, December 2015

[70] S.A. Ansari, M. Asif, T. Rashid, K.G. Qasim, “Burnup studies of spent fuels of vayring types and enrichment”, Annals of Nuclear Energy 34 (2007) 641 – 651

[71] Mariano Vela Mora, Alebrto Gallardo Padilla, José Luis Castro Palomino, “Nondestructive burnup measurements by gamma-ray spectroscopy on spent fuel elements of the RP-10 research reactor”, Progress in Nuclear Energy, 53 (2011) 344 - 353

[72] Michal Koleška, Ladislav Viererbl, Milan Marek, Jaroslov Ernest, Michal Šunka, “Determination of IRT-2M fuel burnup by gamma spectroscopy”, Applied Radiation and Isotopes, 107 (2016) 92 – 97;

[73] Sung-Ho Eom, Hee-Moon Kim, Seung-Je Baik, Sang-Bok Ahn, “Status of the Gamma Scanning Techniques for the Spent PWR Fuel in KAERI-PIEF”, Transactions of the Korean Nuclear Society Spring Meeting, Jeju, Korea, May 10 – 11, 2007

[74] Peter Jansson, Michael L. Fugate, Andrea Favalli, Stephen J. Tobin, Anders Sjöland and Henrik Liljenfeldt, “Axial and Azimuthal Gamma Scanning of Nuclear Fuel – Implications for Spent Fuel Characterization”, Journal of Nuclear Material Management, 45 (No; 1) (2016) 34 - 47

[75] R. Bernt, “Verification of Spent PWR Fuel Data using the ^{154}Eu, ^{134}Cs and ^{137}Cs Activities”, Kernenergie 31 (1988) 59 - 63

[76] D. K. Min, H.J. Park, K.J. Park, S.G. Ro, H.S. Park, ”Determination of burnup, cooling time and initial enrichment of PWR spent fuel by use of gamma-ray activity ratios”, Proceedings of the International symposium on storage of spent fuel from power reactors; Vienna (Austria); 9-13 November 1998, IAEA-SM-352/9P, pp. 421 - 426

[77] Christofer Willman, Ane Håkansson, Otasowie Osifo, Anders Bäcklin, Staffan Jacobsson Svärd, “Nondesctructive assay of spent nuclear fuel with gamma-ray spectroscopy”, Annals of Nuclear Energy “” (2006) 427 - 438

[78] Péter Kirchknopf, Istváv Almási, Gábor Radócz, Imre Nemes, Péter Völgyesi, Imre Szalóki, “Determining burnup, cooling time and operational history of VVER-440 spent fuel assemblies based on in-situ gamma spectrometry at Paks Nuclear Power Plant”, Annals of Nuclear Energy 170 (2022) 108975

[79] S. Vaccaro, S.J. Tobin, A. Favalli, B. Grogan, P. Jansson, H. Liljenfeldt, V. Mozin, J. Hu, P. Schwalbach, A. Sjöland, H. Trellue and D. Vo, “PWR and BWR spent fuel assembly gamma spectra measurements", Nuclear Instruments and Methods in Physics Research A 833 (2016) 208–225

[80] P. Schillebeeckx, A. Borella, M. Bruggeman and R. Rossa, “Cadmium Zinc Telluride Detectors for Safeguards Applications”, in Advanced Materials for Radiation Detectors, Editor K. Iniewski, Springer Nature Switzerland, pp. 331 – 346 (2022)

[81] A. Leburn, G. Bignan, J.L. Szabo, J. Arenas-Carrasco, R. Arlt, A. Dubreuil, and K. Esmailpur Kazerouni, “Gamma spectrometric characterisation of short cooling time nuclear spent fuels using hemispheric CdZnTe detectors”, Nucl. Instr. Meth. Phys. Res. A 448 (2000) 598 - 603

[82] R. Berndt and P. Mortreau, “Spent-fuel characterization with small CZT detectors”, Nuclear Instruments and Methods in Physics Research A 564 (2006) 290 – 294

[83] P. Jansson, M. Bengtsson, U. Bäckström, S. Grape, E. Branger, A. Sjöland., ”Time stamped list mode data from gamma-ray spectroscopic measurements on 47 nuclear fuel assemblies performed at Clab, Sweden, September 2016 through March 2019”. Data Brief 31 (2019) 106039.

[84] M. Bengtsson, Peter Jansson, Ulrika Bäckstrom, Fredrik Johanssson & Anders Sjöland, “Experimental Method for Verification of Calculated ^{137}Cs Content in Nuclear Fuel Assemblies”, Nuclear Technology 208 (2022) 295 - 302

[85] Virginie Solans, Henrik Sjöstrand, Peter Jansson, Peter Schillebeeckx, Sophie Grape, Erik Branger and Anders Sjöstrand, “Spent Nuclear Fuel passive gamma analysis and reproducibility: Application to SKB-50 assemblies”, Annals of Nuclear Energy 192 (2023) 109941

[86] J. L. Parker and T. D. Reilly, “Plutonium Isotopic Determination by Gamma-Ray Spectroscopy,” in Nuclear Analysis Research and Development Program Status Report, January-April 1974, G. Robert Keepin, Ed., Los Alamos Scientific Laboratory report LA-5675-PR (August 1974).

[87] J.R. Phillips, G.E. Bosler, J.K. Halbig, S. F. Klosterbuer, H.O. Menlove, P.M. Rinard, “Experience using a spent fuel measurement system”, Nuclear Materials Management XII (1983) 175– 181.

[88] P.M. Rinard and G.E. Bosler, Safeguarding LWR Spent Fuel with the Fork Detector, Report LA – 11096 – MS, Los Alamos National Laboratory, March 1988

[89] G.E. Bosler and P.M. Rinard, “Burnup measurements with the Los Alamos FORK detector”, Report LA-UR-91-2508, December 1991.

[90] A. Tiitta, J. Hautamäki, A. Turunen, R. Arlt, J.A. Carrasco, K. Esmailpour-Kazerouni, P. Schwalbach, "Spent BWR fuel characterisation combining a FORK detector with gamma spectrometry, Report STUK-YTO-TR 175, February 2001

[91] A. Borella, R. Carchon, C. DeLimelette, D. Symens and K. van der Meer, “Spent Fuel Measurements with the Fork Detector at the Nuclear Power Plant of Doel”, in *ESARDA 33rd annual meeting.* Luxembourg, 2011 - ESARDA - European Safeguards Research & Development Association, Budapest, Hungary, 2011-05-16.

[92] A. Borella and K. van der Meer, “The Fork Detector for Spent Fuel Measurements: Measurements and Simulations”, in *Proceeding of the 53rd INMM Annual Meeting,* 15-19 July, 2012, Orlando, Florida, USA.

[93] Riccardo Rossa and Alessandro Borella, “Development of the SCK CEN reference datasets for spent fuel safeguards research and development”, Data in Brief 30 (2020) 105462

[94] Tomas Martinik, Vladimir Henzl, Sophie Grape, Peter Jansson, Martyn T. Swinhoe, Alison V. Goodsell and Stephen J. Tobin, "Design of a prototype Differential Die-Away instrument proposed for Swedisch spent nuclear fuel characterization", Nuclear Instruments and Methods in Physics Research A 821 (2016) 55 – 65

[95] Cole Thompson, Garreth McMath, Ulrika Bäckström, William S. Charlton, Vlad Henzl, Paul Mendoza, Carlos Rael, Margaret Roor, Anders Sjöland, Alexis Trahan and Holly R. Trellue, “Improved evaluation of safeguards parameters from spent fuel measurements with the Differential Die-Away (DDA) instrument”, Nuclear Instruments and Methods in Physics Research A 1029 (2022) 166462

[96] H.O. Menlove, S.H. Menlove and S.J. Tobin, "Fissile and fertile nuclear material measurements using a new differential die-away-self-interrogation technique", Nuclear Instruments and Methods in Physics Research A 602 (2009) 588 – 593

[97] Alexis C. Kaplan, Vladimir Henzl, Howard O. Menlove, Martyn T. Swinhoe, Anthony P. Belian, Marek Flaska and Sara A. Pozzi, "Determination of total plutonium content in spent nuclear fuel assemblies with the differential die-away self-interrogation instrument", Nuclear Instruments and Methods in Physics Research A 764 (2014) 347 – 351

[98] Alexis C. Trahan, Garrett E. McMath, Paul M. Mendoza, Holly R. Trellue, Ulrika Backstrom, Li Pöder Balkeståhl, Sophie Grape, Vlad Henzl, Daniel Leyba, Margaret A. Root and Anders Sjoland, “Results of the Swedish spent fuel measurement field trials with the Differential Die-Away Self-Interrogation Instrument”, Nuclear Instruments and Methods in Physics Research A 795 (2020) 163329

[99] V. Solans et al. “Rossi-Alpha distribution analysis of DDSI data for spent nuclear fuel investigation”. Symposium on International Safeguards: Reflecting on the Past and Anticipating the Future, IAEA Vienna (2022)

[100] D.M. Lee and L.O. Lindqvist, "Self-interrogation of spent fuel", Report LA-9494-MS, August 1982

[101] Alan Michael Bolind, "Development of an analytical theory to describe the PNAR and CIPN nondestructive assay techniques", Annals of Nuclear Energy 66 (2014) 167 – 176

[102] J. Eigenbrodt, S.J. Tobin, W.S. Charlton, A.M. Bolind, H.O. Menlove, M. Seya, and H.R. Trellue, "PNAR Measurements of Fugen Fuel", 55th Annual Meeting of the Institute of Nuclear Materials Management, Atlanta, Georgia, 20-14 July 2014

[103] J. Eigenbrodt, and H.O. Menlove, “Spent Fuel Measurements: Passive Neutron Albedo Reactivity (PNAR) and Photon signatures", Los Alamos Report, LA–UR–16–22112,March 2016

[104] Stephen Joseph Tobin, Topi Tupasela, Peter Dendooven and Tapani Honkamaa, "PNAR measurement report", Report LA-UR-19-30861, October 2019

[105] S.J. Tobin, P. Peura, C. Bélanger-Champagne, M. Moring, P. Dendooven and T. Honkama, Measuring spent fuel assembly multiplication in borated water with a passive neutron albedo reactivity instrument, Nuclear Instruments and Methods in Physics Research A 897 (2018) 32 – 37